AD-A120 187 MITRE CORP MCLEAN VA METREK DIV F/G 17/7
CONFLICT MONITORING ANALYSIS OF PARALLEL OPPOSITE DIRECTION ROU--ETC(U)
AUG 82 A P SMITH DTFA01-82-C-10003
UNCLASSIFIED MTR-82W00114-VOL-2 FAA-EM-82-23-VOL-2 NL

1 OF 1
AD A
120187

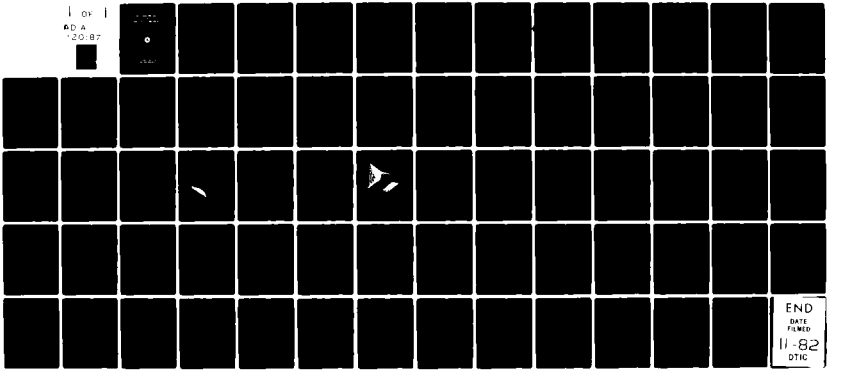

END
DATE FILMED
11-82
DTIC

Report No. FAA-EM-82-23
Volume II

MTR-82W114
Volume II

12

CONFLICT MONITORING ANALYSIS OF PARALLEL OPPOSITE DIRECTION ROUTES

Arthur P. Smith, III

The MITRE Corporation
McLean, Virginia 22102

AUGUST 1982

Prepared for

U.S. DEPARTMENT OF TRANSPORTATION
FEDERAL AVIATION ADMINISTRATION
OFFICE OF SYSTEMS ENGINEERING MANAGEMENT
Washington, D.C. 20591

Technical Report Documentation Page

1. Report No.	2. Government Accession No.	3. Recipient's Catalog No.
FAA-EM-82-23	AD-A120 187	

4. Title and Subtitle
Conflict Monitoring Analysis of Parallel Opposite Direction Routes

5. Report Date
August 1982

6. Performing Organization Code

7. Author(s)
Arthur P. Smith, III

8. Performing Organization Report No.
MTR-82W00114, Volume II

9. Performing Organization Name and Address
The MITRE Corporation
Metrek Division
1820 Dolley Madison Boulevard
McLean, Virginia 22102

10. Work Unit No. (TRAIS)

11. Contract or Grant No.
DTFA01-82-C10003

12. Sponsoring Agency Name and Address
Office of Systems Engineering Management
Federal Aviation Administration
Department of Transportation
Washington, D.C. 20591

13. Type of Report and Period Covered

14. Sponsoring Agency Code
DOT/FAA

15. Supplementary Notes

16. Abstract

This paper reports on the development of the Conflict Monitoring Analysis. A previous report (FAA-EM-80-16) described the estimates of the probability of horizontal overlap and controller intervention rate for same direction adjacent parallel routes. This work extends that methodology to opposite direction adjacent parallel routes. For both the probability of horizontal overlap and the controller intervention rate, trial results based on data are given.

17. Key Words	18. Distribution Statement
Collision Risk Methodology Safety Controller Intervention Rate VOR Route Spacing Aircraft Separation	Document is available to the public through the National Technical Information Service, Springfield, VA 22161

19. Security Classif. (of this report)	20. Security Classif. (of this page)	21. No. of Pages	22. Price
Unclassified	Unclassified		

Form DOT F 1700.7 (8-72) Reproduction of completed page authorized

TABLE OF CONTENTS

LIST OF ILLUSTRATIONS

LIST OF ILLUSTRATIONS
(Continued)

1. INTRODUCTION

The first volume of this report presents results of the work to extend the Conflict Monitoring Analysis to opposite direction traffic flows at the same flight levels for parallel routes. The appendices in this volume present the details of the opposite direction analysis. As pointed out in Volume I, much of the supporting analysis for the opposite direction study is common to the earlier study of same direction routes and can be found in Volume II of Reference 3. The appendices in this volume address the analytical differences between same and opposite direction traffic flows. The specific topics discussed in this volume are described below:

- Some initial work to address conflicts involving turning aircraft was done in the opposite direction analysis. Appendix A describes the accelerations observed in the data.

- In the same direction analysis, errors in the estimates of the crosstrack separations and closing speeds were considered. In the opposite direction analysis, the alongtrack dimension also becomes important since the closing speed is largely in that dimension. Appendix B addresses the surveillance system and tracker errors which contribute to the errors in the estimates of the crosstrack and alongtrack separation and closing speeds.

- By considering both the crosstrack and alongtrack dimensions in the opposite direction analysis, the description of the conflict region is also modified from the same direction analysis. Appendix C describes the opposite direction conflict surface. As in the same direction analysis the delay incurred before the controller realizes that the aircraft pair is within the conflict region is required. Appendix D addresses the computation of the delay for the opposite direction conflict region.

- In the same direction analysis the aircraft performing the resolution maneuver was assumed to turn toward its assigned route centerline. In the high closure rate situation of opposite direction traffic flow this maneuver may not be the most effective. Appendix E desribes the Conflict Resolution Advisory which is

being developed for NAS and is used in the opposite direction Conflict Monitoring Analysis as the logic for selecting the resolution maneuver.

- The net result of the Conflict Monitoring Analysis is to estimate the probability of horizontal overlap. The inclusion of acceleration and both left and right turns for resolutions means that there are new descriptions of the overlap regions in the opposite direction analysis. These are discussed in Appendix F.

- The combination of all the appropriate probabilities to arrive at the estimate of the probability of horizontal overlap is addressed in Appendix G.

An indication of the parts of the opposite direction analysis that use the results from these appendices is given in Figure 1-1.

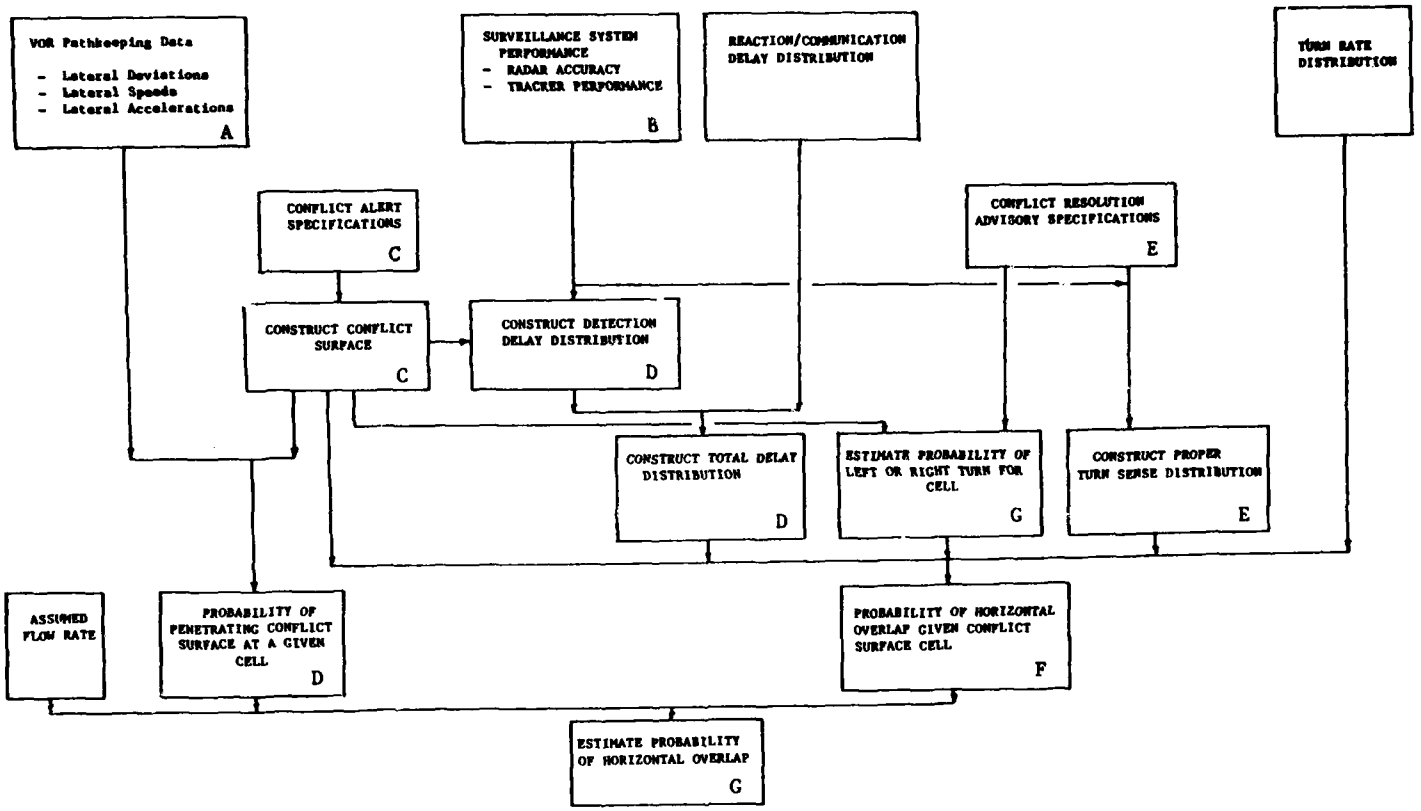

FIGURE 1-1
OVERVIEW OF THE ROUTE SPACING ANALYSIS FOR OPPOSITE DIRECTION TRAFFIC FLOWS

APPENDIX A

AVERAGE RELATIVE LATERAL ACCELERATIONS

Even though the opposite direction Conflict Monitoring Analysis is not developed to the point of making satisficatory estimates of horizontal overlap probability with accelerated flight trajectories, this appendix will document the accelerations found in one sample of flight tracks. In particular it is of interest to examine the relative lateral (crosstrack) accelerations averaged over a two minute period. The averaging is desired because the conflict encounter lasts about two minutes or until the aircraft pass. Furthermore, an average acceleration estimate is a more stable estimate than an instantaneous acceleration estimate made from position reports.

The average acceleration estimates were made by considering 184 aircraft tracks on jet route J146 in Cleveland. The data available were the crosstrack deviations from the route centerline at twelve second time intervals. This set of points was smoothed with a cubic spline function. Between data points i and i+1 the spline function is defined as

$$y_i = A_i + B_i(t-t_i) + C_i(t-t_i)^2 + D_i(t-t_i)^3 \qquad t_i \leq t < t_{i+1} \qquad \text{(A-1)}$$

such that y and its first and second derivatives are continuous at each point. The technique used here is called spline function smoothing (Reference 2) where the objective is to minimize the second derivative of the function over the entire interval.

Given the crosstrack deviation between each pair of points given by (A-1) the average crosstrack acceleration between point i and point i+1 is

$$\bar{a}_i = 2C_i + 3D_i\,(t_{i+1} - t_i) \qquad \text{(A-2)}$$

In this case $t_{i+1} - t_i$ is equal to 12 seconds. After the average lateral acceleration is computed over each 12 second interval an average over ten 12 second intervals (2 minutes) is taken. After a gap of two minutes in the track another two minute average is taken. The resulting histogram of average lateral accelerations for single aircraft is shown in Figure A-1. Although the samples in the histogram are not truly independent they will be considered as such for the purposes of this analysis.

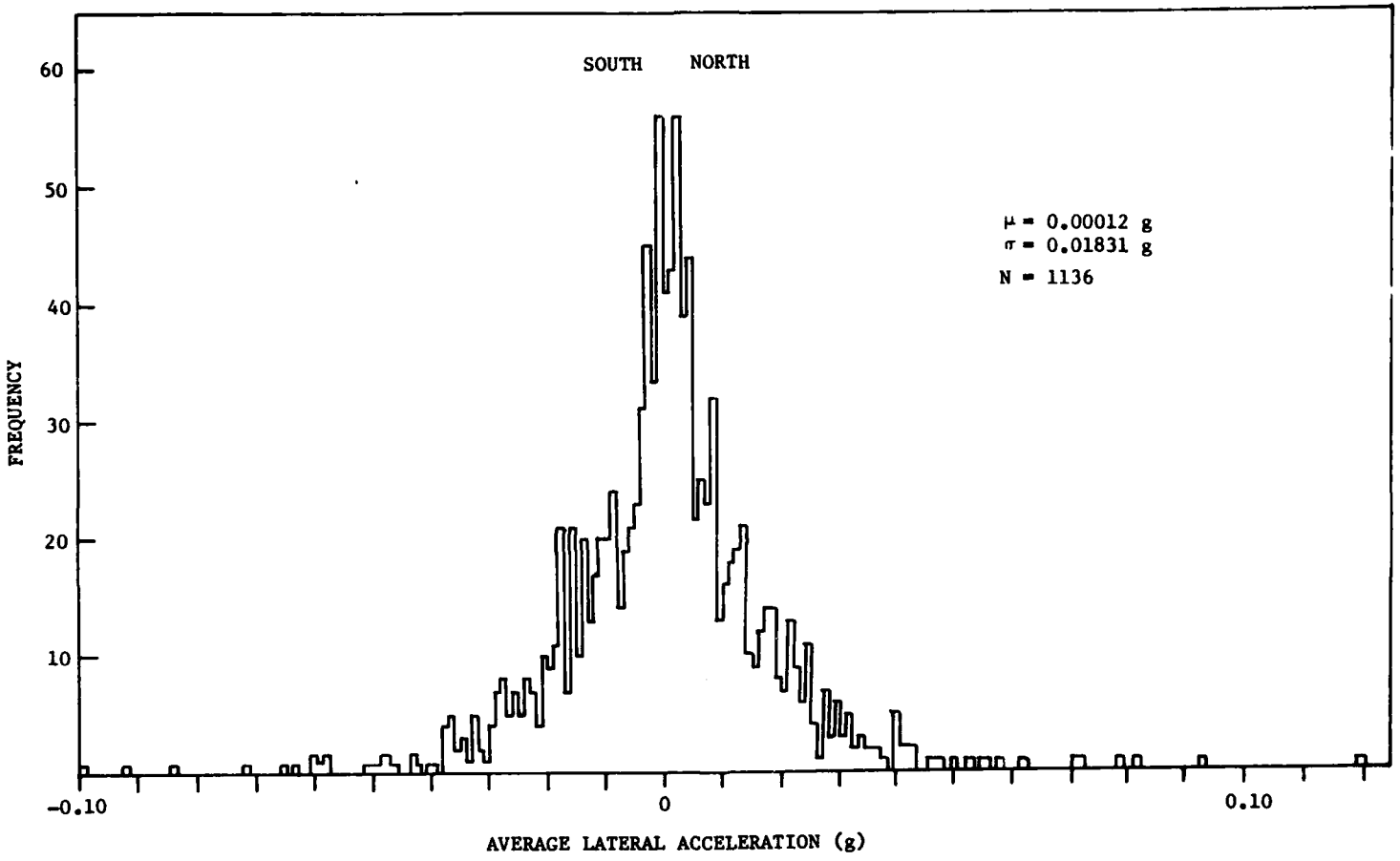

FIGURE A-1
SINGLE AIRCRAFT AVERAGE
LATERAL ACCELERATION

Since the relative lateral acceleration is required, the histogram in Figure A-1 was convolved with itself using the Fast Fourier Transform (see Appendix D of Volume II of Reference 3). The resulting histogram which was presented in Volume I of this report is shown in Figure A-2.

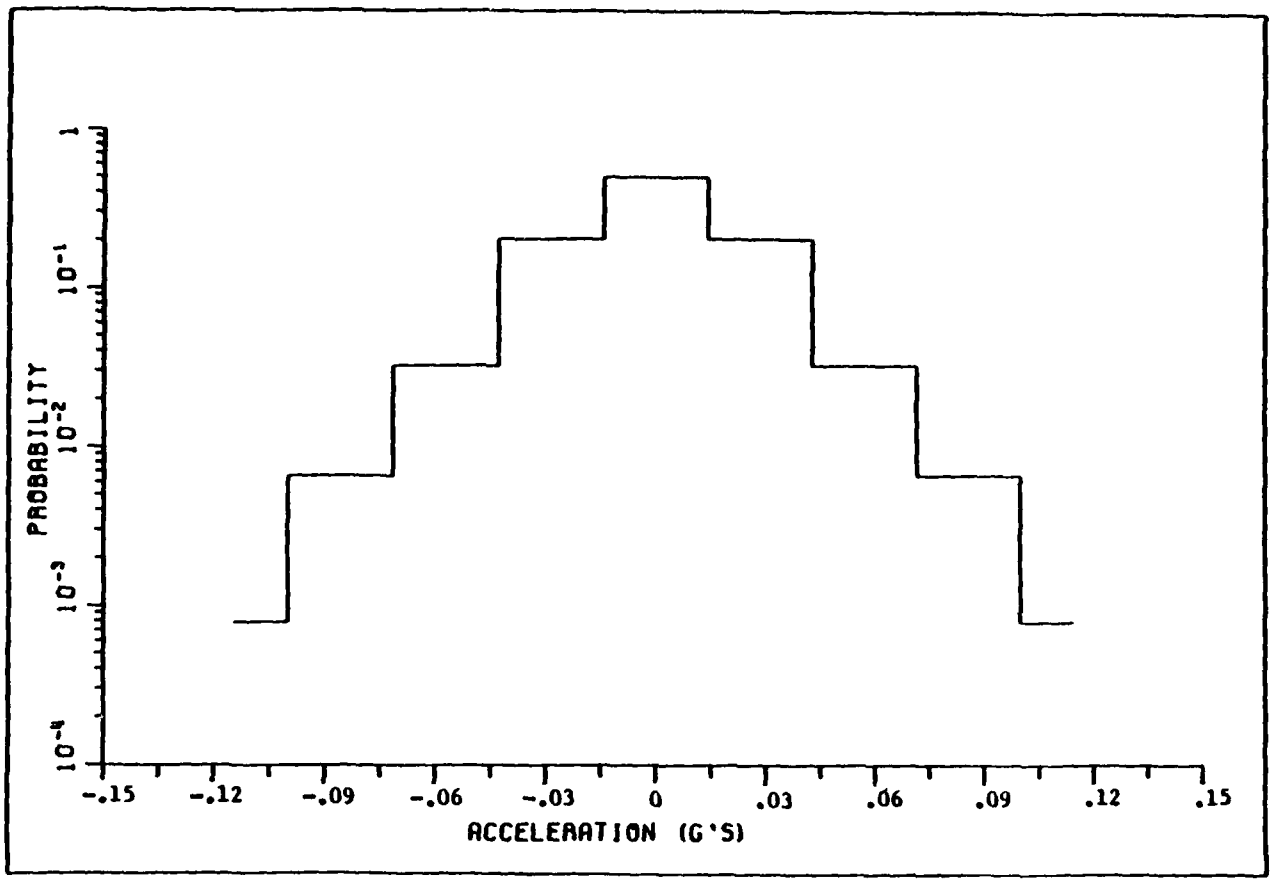

FIGURE A-2
AVERAGE RELATIVE CROSSTRACK
ACCELERATION HISTOGRAM

APPENDIX B

SURVEILLANCE/TRACKER ERRORS

B.1 Background

In the same direction Conflict Monitoring Analysis we needed to know the probability of observing the aircraft pair outside the conflict boundary when the aircraft pair was truly inside the boundary. The uncertainty of observing the aircraft pair inside or outside the conflict boundary is due to the errors in the surveillance/tracking system. It was assumed in the same direction case that the errors in the crosstrack closing speed and the crosstrack separation were sufficient to describe the situation . Therefore the estimate of the probability of observing the aircraft pair outside the conflict boundary when it was truly inside was made using an approximation for the volume under a correlated bivariate normal distribution. The procedure for making that estimate is discussed in Appendix C of Volume II of Reference 3.

In the opposite direction Conflict Monitoring Analysis there is an analogous need for the probability of being observed outside the conflict boundary when the aircraft pair is truly inside the boundary. However, in the opposite direction case the errors in the alongtrack separation and the crosstrack speed of one of the aircraft due to the surveillance/tracking system are also important. Therefore the probability of observing a conflicting pair outside the conflict surface will be estimated using a correlated quadrivariate normal distribution.

This appendix will discuss how the parameters of the quadrivariate normal distribution were arrived at. This is followed by a discussion of how one can randomly sample from a correlated quadrivariate normal distribution.

B.2 Parameter Estimation

The parameter of the correlated quadrivariate normal distribution were estimated via simulation. The simulation was run for four orientations of the parallel routes with respect to the radar. In each case 15 pairs of aircraft were flown down the routes. The aircraft tracks came from the FAA's VOR navigation data base. There were 200 randomly chosen tracks from the selected routes in the Cleveland ARTCC. From two opposite direction routes 50 aircraft were chosen to comprise

the population (approximately 25 aircraft on each route). In the simulation the pairs of aircraft were chosen from their respective route populations. These pairs were chosen with replacement. The aircraft were placed on their respective routes within 5 nmi alongtrack of the designated starting points of the routes. The aircraft were allowed to travel approximately 10 nmi before statistics were taken. This allowed for the transients in the tracker to die out. Figure B-1 shows the configurations of the four cases.

The errors in the surveillance system were modelled in the following manner. It was assumed that the azimuth error was normally distributed, mean of zero and standard deviation of 0.264 degrees (3 ACPs). The range error is a combination of two errors. The first is a bias error built into the airborne transponder. This is assumed to be uniformly distributed between $\pm$ 0.5 of a microsecond ($\pm$ 0.08 nmi). This error is assigned to each aircraft as it enters the simulation. The second range error is due to the range quantization in the common digitizer. The quantization is 1/8 nmi and the error is applied at each radar update. The probability of a radar return (blip/scan) is set at 0.95.

Each track contains the information about the position and velocity of the aircraft at each update time. At each update the "true" position and velocity components are compared to the "observed" position and velocity components. Positive values for the variables have the following meanings:

Alongtrack separation (x) -- the aircraft appear to be farther apart than they truly are,

Crosstrack separation (y) -- the aircraft appear to be farther apart than they truly are,

Crosstrack closing speed ($\dot{y}$) -- the aircraft appear to be closing faster than they truly are,

Crosstrack speed of aircraft 1 ($\dot{y}_1$) -- the aircraft appears to be flying north faster than it truly is.

The results for the sixty pairs of aircraft (15 pairs times 4 route orientations) are given in Tables B-1, B-2, and B-3.

UX is the estimate of the mean alongtrack separation error,

UY is the estimate of the mean crosstrack separation error,

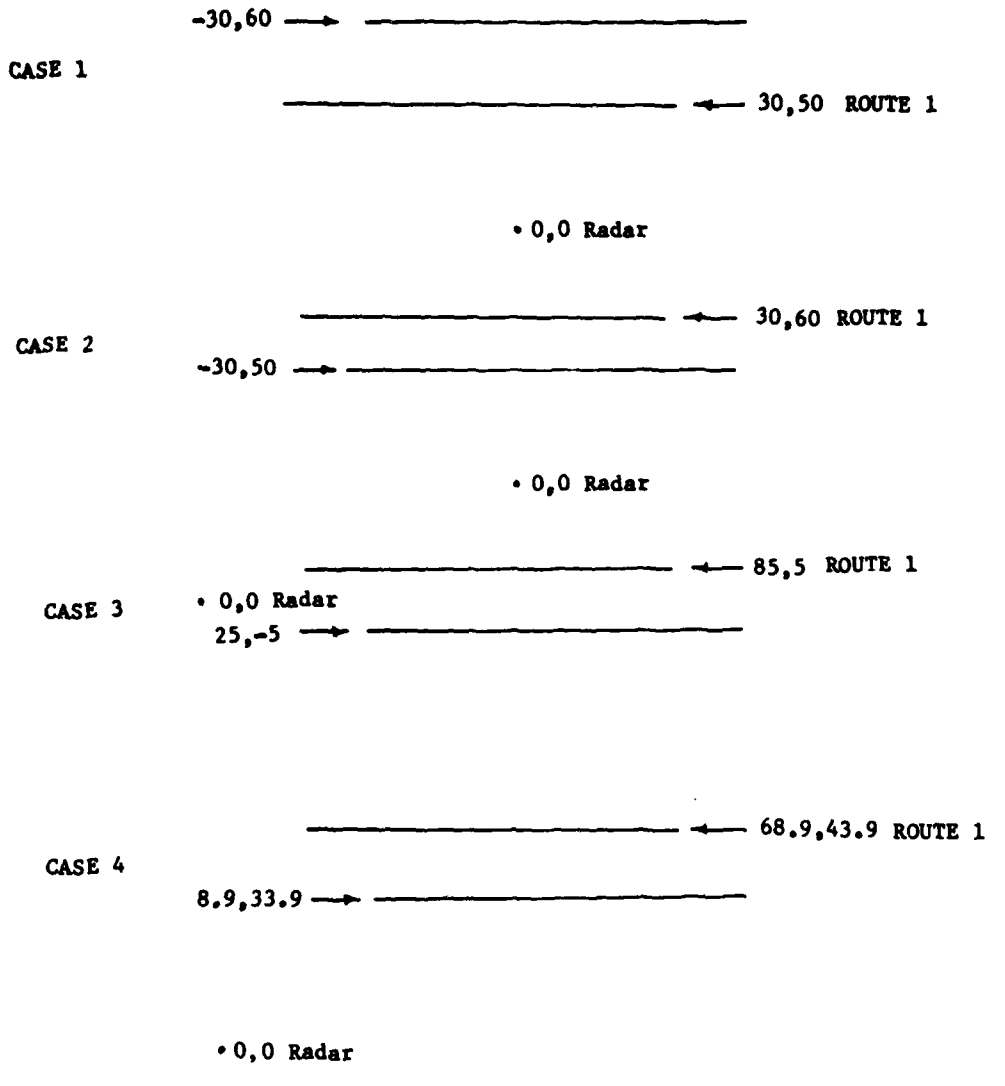

FIGURE B-1
ROUTE CONFIGURATIONS RELATIVE
TO THE RADAR

TABLE B-1

ESTIMATES OF MEANS
SURVEILLANCE/TRACKER ERRORS

Case		μ_x	μ_y	$\mu_{\dot{y}}$	$\mu_{\dot{y}_1}$
1	μ	-0.063	0.147	-20.595	-11.305
	σ	0.116	0.242	42.371	17.934
2	μ	-0.095	-0.029	9.549	-8.666
	σ	0.152	0.194	30.905	13.018
3	μ	-0.126	-0.119	21.035	-2.580
	σ	0.087	0.219	24.508	12.403
4	μ	-0.143	-0.090	20.264	-2.618
	σ	0.109	0.177	22.624	11.628
Total	μ	-0.107	-0.023	7.565	-6.294
	σ	0.119	0.229	34.731	14.138
Accept Reject		R	A	A	R

H0 : $E(\mu)=0$
$\alpha = 0.05$

TABLE B-2

ESTIMATES OF STANDARD DEVIATIONS
SURVEILLANCE/TRACKER ERRORS

Case		σ_x	σ_y	$\sigma_{\dot{y}}$	$\sigma_{\dot{y}_1}$
1	μ	0.305	0.285	45.850	28.758
	σ	0.061	0.117	18.270	14.932
2	μ	0.403	0.194	30.513	19.224
	σ	0.137	0.089	12.316	12.901
3	μ	0.250	0.327	40.058	22.181
	σ	0.085	0.163	18.649	11.171
4	μ	0.307	0.305	40.823	22.337
	σ	0.152	0.160	17.521	12.322
Total	μ	0.316	0.278	39.310	23.128
	σ	0.125	0.142	17.374	13.052

TABLE B-3

ESTIMATES OF CORRELATIONS
BETWEEN
SURVEILLANCE/TRACKER ERRORS

Case		ρ_{xy}	$\rho_{x\dot{y}}$	$\rho_{x\dot{y}_1}$	$\rho_{y\dot{y}}$	$\rho_{y\dot{y}_1}$	$\rho_{\dot{y}\dot{y}_1}$
1	μ	0.012	-0.075	0.185	-0.658	-0.590	0.672
	σ	0.386	0.419	0.372	0.177	0.263	0.273
2	μ	0.058	-0.002	0.177	-0.594	-0.350	0.464
	σ	0.380	0.308	0.357	0.188	0.480	0.389
3	μ	0.007	-0.142	-0.082	-0.558	-0.307	0.501
	σ	0.488	0.424	0.497	0.282	0.445	0.367
4	μ	0.246	-0.276	-0.018	-0.623	-0.294	0.521
	σ	0.391	0.328	0.423	0.232	0.469	0.347
Total	μ	0.098	-0.124	0.066	-0.608	-0.385	0.539
	σ	0.413	0.378	0.422	0.221	0.431	0.347
Accept Reject		A	R	A	R	R	R

H0 : $E(\rho)=0$
$\alpha = 0.05$

UYD is the estimate of the mean crosstrack closing speed error,

UYD1 is the estimate of the mean crosstrack speed error of aircraft one,

SX, SY, SYD, SYD1 are the estimates of the corresponding one sigma values.

PXY is the estimate of the correlation coefficient between the alongtrack and crosstrack separation errors,

PXYD is the estimate of the correlation coefficient between the alongtrack separation and the crosstrack closing speed errors,

PXYD1 is the estimate of the correlation coefficient between the alongtrack separation and the crosstrack speed of aircraft one errors,

PYYD is the estimate of the correlation coefficient between the crosstrack separation and the crosstrack closing speed errors,

PYYD1 is the estimate of the correlation coefficient between the crosstrack separation and the crosstrack speed of aircraft one errors,

PYDYD1 is the estimate of the correlation coefficient between the crosstrack closing speed and the crosstrack speed of aircraft one errors.

Table B-1 shows the mean and standard deviations of the mean errors. Assuming the means are distributed normally, a t-test could be used to test the hypothesis that the means have been sampled from a population with a zero mean. Even though two of the t-tests would statistically reject the hypothesis of zero means, operationally the means are near enough to zero that a value of zero will be used in the analysis.

Table B-2 shows the means and standard deviations of the standard deviation of the errors. For both the alongtrack and crosstrack separation errors the standard deviation is estimated to be about 0.3 nmi. The standard deviation of the crosstrack closing speed error is about 39 kts. The standard deviation of the crosstrack speed of aircraft one is about 23 kts.

Table B-3 shows the means and standard deviations of the pairwise correlation coefficients. If normality is assumed, a t-test could be used to test the hypothesis that the crosstrack errors are uncorrelated. This test shows that the alongtrack dimension is basically uncorrelated with the crosstrack dimension. This is reasonable since the computation of the crosstrack velocities is based only on the crosstrack positions and the crosstrack errors are uncorrelated with the alongtrack errors.

Thus, for the purposes of the Conflict Monitoring Analysis, the quadrivariate normal distribution parameters listed in Table B-4 are used to specify the surveillance/tracker errors for a pair of opposite direction aircraft.

B.3 Sampling From a Quadrivariate Normal Distribution

In the determination of detection delays (Appendix D of this paper) it will be necessary to sample from a correlated quadrivariate normal distribution. The reason this is necessary is that there is no general approximation for a volume under such a distribution.

If $U_1, U_2 \ldots, U_m$ are independent unit normal variables their joint density is

$$P_u(\underline{U}) = (2\pi)^{-(1/2)^m} \exp\left[-\frac{1}{2} \sum_{j=1}^{m} U_j^2 \right]$$

$$= (2\pi)^{-(1/2)^m} \exp\left(-\frac{1}{2} \underline{U}^T \underline{U} \right).$$

If we apply a nonsingular linear transformation, to

$\underline{Y}^T = (Y_1, \ldots, Y_m)$,

$$\underline{U}^T = \underline{Y}^T \underline{\underline{H}}^T \text{ with } |\underline{\underline{H}}| \neq 0, \qquad \text{(B-1)}$$

TABLE B-4

PARAMETER VALUES
OF THE
QUADRIVARIATE SURVEILLANCE/TRACKER
ERROR DISTRIBUTION

Parameter	Value
μ_x	0 nmi
μ_y	0 nmi
$\mu_{\dot{y}}$	0 kts
$\mu_{\dot{y}_1}$	0 kts
σ_x	0.3 nmi
σ_y	0.3 nmi
$\sigma_{\dot{y}}$	39 kts
$\sigma_{\dot{y}_1}$	23 kts
$\rho_{x\dot{y}}$	0
$\rho_{x\dot{y}}$	0
$\rho_{x\dot{y}_1}$	0
$\rho_{y\dot{y}}$	-0.6
$\rho_{y\dot{y}_1}$	-0.4 (Route 1 North of Route 2)
$\rho_{\dot{y}\dot{y}_1}$	0.5 (Route 1 North of Route 2)

we find that $\underline{Y}$ has a joint density function

$$p_y(\underline{y}) = (2\pi)^{-(\frac{1}{2})m}|\underline{\underline{H}}| \exp(-\tfrac{1}{2}\underline{y}^T \underline{\underline{H}}^T \underline{\underline{H}}\,\underline{y})$$
$$= (2\pi)^{-(\frac{1}{2})m}|\underline{\underline{R}}|^{\frac{1}{2}}\exp(-\tfrac{1}{2}\underline{y}^T \underline{\underline{R}}\,\underline{y}) \qquad \text{(B-2)}$$

where $\underline{\underline{R}}=\underline{\underline{H}}^T\underline{\underline{H}}$ is positive definite.
The variance-covariance matrix of $\underline{Y}$ is $\underline{\underline{R}}^{-1}$. Since the correlation coefficient is related directly to the covariance

$$\rho_{xy} = \frac{\sigma xy}{\sigma x\, \sigma y}$$

We see that a matrix of the form

$$\underline{\underline{\rho}} = \begin{bmatrix} 1 & \cdot & \cdot & \cdot & \rho_{1m} \\ \cdot & & & & \cdot \\ \cdot & & & & \cdot \\ \cdot & & & & \cdot \\ \rho_{m1} & \cdot & \cdot & \cdot & 1 \end{bmatrix}$$

can represent the symmetry of $\underline{\underline{R}}^{-1}$. Thus, knowing $\underline{\underline{\rho}}$ we can invert to find $\underline{\underline{R}}$. Knowing $\underline{\underline{R}}$ we solve $\underline{\underline{R}} = \underline{\underline{H}}^T\underline{\underline{H}}$ to find $\underline{\underline{H}}$. Then knowing $\underline{\underline{H}}$ we will know the transformation to convert the independent unit normal variables ($\underline{U}$) to the correlated variables ($\underline{Y}$):

$$\underline{U}^T(\underline{\underline{H}}^T)^{-1}=\underline{Y}^T.$$

Inverting ρ to find $\underline{\underline{R}}$ is straightforward. The solution of (B-2) is accomplished by a Cholesky decomposition which is a matrix manipulation supported by "SAS" (the Statistical Analysis System computer program package).

As an example of the generation of a correlated quadrivariate random numbers consider four variables: x, y, $\dot{y}$, and $\dot{y}_1$. Assume that x is independent of the other variables. Let the ρ matrix be

$$\underline{\underline{\rho}} = \begin{bmatrix} 1 & 0 & 0 & 0 \\ 0 & 1 & -0.66 & 0.59 \\ 0 & -0.66 & 1 & -0.67 \\ 0 & 0.59 & -0.67 & 1 \end{bmatrix}$$

The resulting matrix $(\underline{\underline{H}}^T)^{-1}$ is

$$(\underline{\underline{H}}^T)^{-1} = \begin{bmatrix} 1 & 0 & 0 & 0 \\ 0 & 0.724400 & 0 & 0 \\ 0 & -0.356565 & 0.742361 & 0 \\ 0 & 0.590000 & -0.670000 & 1 \end{bmatrix}$$

This means that

$$\underline{Y} \begin{cases} x = U_1 \sigma_x \\ y = (0.7244\ U_2 - 0.356565\ U_3 + 0.59\ U_4)\ \sigma_y \\ \dot{y} = (0.742361 U_3 - 0.67\ U_4\ )\ \sigma_{\dot{y}} \\ \dot{y}_1 = U_4\ \sigma_{\dot{y}_1} \end{cases} \qquad \text{(B-3)}$$

where U_i are unit normal random numbers and σ_i are the standard deviations of each variable. If $\sigma_x = 1$, $\sigma_y = 2$, $\sigma_{\dot{y}} = 3$, and $\sigma_{\dot{y}_1} = 4$ and a Monte Carlo simulation is run 150 times picking x, y, $\dot{y}$, and $\dot{y}_1$, according to (B-3) the results are:

Variable	Mean	Standard Deviation
x	-0.0009 (0)	0.98 (1)
y	0.0741 (0)	2.22 (2)
$\dot{y}$	-0.4276 (0)	3.01 (3)
$\dot{y}_1$	0.5819 (0)	4.00 (4)

Correlation Coefficents

ρ_{xy}	=-0.022 (0)
$\rho_{x\dot{y}}$	=-0.033 (0)
$\rho_{x\dot{y}_1}$	= 0.087 (0)
$\rho_{y\dot{y}}$	=-0.709 (-0.66)
$\rho_{y\dot{y}_1}$	= 0.609 (0.59)
$\rho_{\dot{y}\dot{y}_1}$	=-0.678 (-0.67)

when the values in parentheses are the parameters of the distribution being sampled from.

APPENDIX C

THE CONFLICT SURFACE

This appendix will develop the analysis necessary to describe the conflict surface for opposite direction traffic. The conflict surface is defined by those values of the separation and closing speed between two aircraft which, when rectilinearly projected ahead in time, would indicate that the aircraft would be separated by 5 nmi in 2 minutes or less. Just outside such a conflict surface the aircraft would not be projected to be separated by 5 nmi within 2 minutes. To understand the conflict surface it is necessary to define the sign conventions of the parameters and explictly describe the conflict criteria.

C.1 Sign Conventions

The following sign conventions are used in the analysis:

y_1 — crosstrack deviation of aircraft 1. Positive is away from own route toward the other route.

y_2 — crosstrack deviation of aircraft 2. Positive is away from own route toward the other route.

y — crosstrack separation = $RS-(y_1 + y_2)$ where RS is the route spacing. Positive indicates that the aircraft are oriented with respect to each other in the same way their respective routes are oriented. In other words, if route 2 is north of route 1 and aircraft 2 is north of aircraft 1, then y is positive.

$\dot{y}_1$ — is the crosstrack velocity of aircraft 1. Positive is away from own route toward the other route.

$\dot{y}_2$ — is the crosstrack velocity of aircraft 2. Positive is away from own route toward the other route.

$\dot{y}=\dot{y}_1+\dot{y}_2$ — is the "closing speed" of the aircraft. $\dot{y}$ is positive if aircraft are closing and $y > 0$. $\dot{y}$ is positive if aircraft are opening and $y < 0$.

x_1 is the alongtrack position of aircraft 1. Positive is in direction of flight of aircraft 1. The origin is arbitrary.

x_2 is the alongtrack position of aircraft 2. The reference frame is the same as for aircraft 1.

$x = x_2 - x_1$ is the alongtrack separation. Positive indicates aircraft have not yet passed.

$\dot{x}_1$ is alongtrack velocity of aircraft 1 (+)

$\dot{x}_2$ is alongtrack velocity of aircraft 2 (- if aircraft 2 is flying in a direction opposite that of aircraft 1.)

$\dot{x} = \dot{x}_2 - \dot{x}_1$ is the alongtrack "closing" velocity. Minus means closing if $x_2 > x_1$.

C.2 Conflict Criteria

A pair of aircraft is said to be in potential conflict if the two aircraft are projected to be within 5 nmi (D) within 2 minutes (T). If one projects the aircraft assuming rectilinear motion, one can plot the aircraft separation as a function of time as shown in Figure C-1. If the projected trajectory of the pair goes through the shaded area the pair would be in potential conflict (i.e., at some point in time less than T the separation of the aircraft would be less than D). There is an obvious distinction that one could make between various trajectories — those that do and those that don't pass through the shaded area. There are three types of trajectories that do pass through the shaded area. These are characterized by the time of closest approach (minimum d) of the trajectory. As shown in Figure C-1, the time of closest approach for trajectory 1 is greater than T. Trajectory 2's time to closest approach is less than T and the separation of the aircraft at T is less than D. Trajectory 3's time to closest approach is less than T but the separation is greater than D at time T. In any case, if there is a potential conflict the distance of closest approach is less than D. The converse, however, is not true. A distance of closest approach less than D does not necessarily mean a potential conflict.

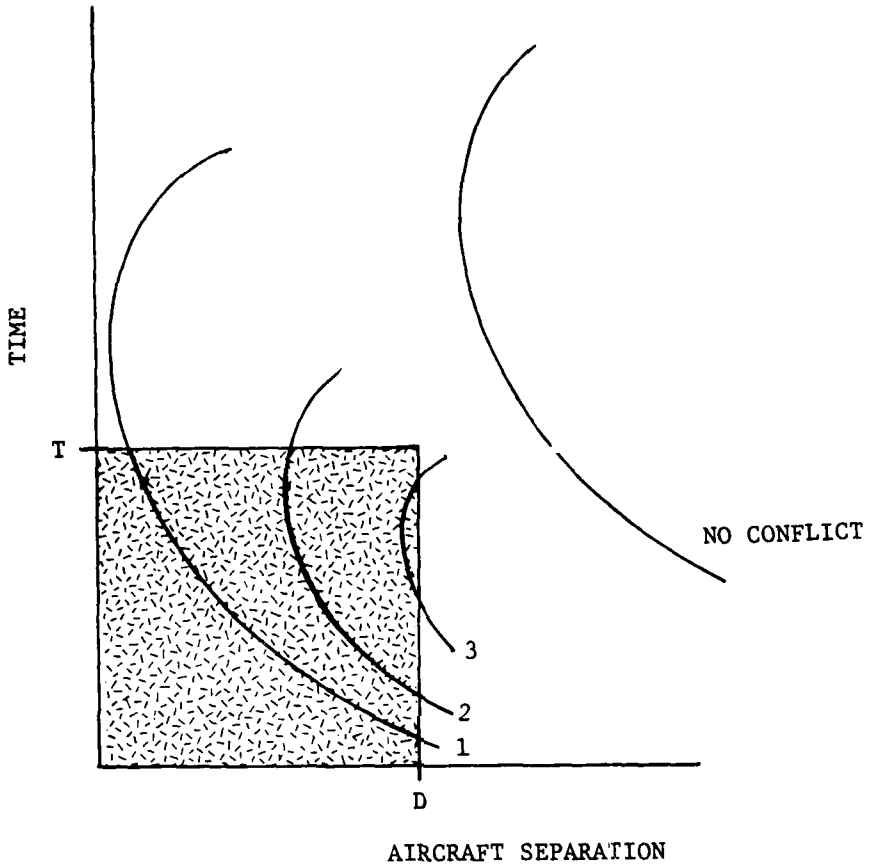

FIGURE C-1
AIRCRAFT SEPARATION TRAJECTORIES

There are three events that one has to consider when determining whether a trajectory is in potential conflict. One event is "the time to closest approach is less than T," ($t_{ca}<T$). The second event is "the distance of closest approach is less than D," ($d_{ca}<D$). The third event is "the distance at time T is less than D," ($d_T<D$). The conflict condition is thus:

$$[(t_{ca}<T) \cap (d_{ca}<D)] \cup (d_T<D). \qquad \text{(C-1)}$$

This logical expression will be used to determine the conflict region boundary in the following analysis.

C.3 Development of the Conflict Boundary

In the development of the conflict boundary it is assumed that the forward speeds of each aircraft are constant and not necessarily equal. Thus, by specifying S_1, S_2, (the two forward speeds), $\dot{y}$, $\dot{y}_1$, x, and y the complete geometry of the encounter is known. This means that $\dot{x}$ is a function of S_1, S_2, $\dot{y}$, and $\dot{y}_1$. Thus, given S_1, S_2, x, $\dot{y}_1$ the conflict geometry is described by y and $\dot{y}$.

If the aircraft are separated at t = 0 by x, y then the aircraft will be separated by

$$d = \sqrt{(x + \dot{x}t)^2 + (y - \dot{y}t)^2} \qquad \text{(C-2)}$$

at time t. This assumes rectilinear motion. From (C-2) one can compute the time to closest approach. It is

$$t_{ca} = (y\dot{y} - x\dot{x}) / (\dot{x}^2 + \dot{y}^2) \qquad \text{(C-3)}$$

If we let $t_{ca} = T$ and solve (C-3) for y we get

$$y = (T(\dot{x}^2 + \dot{y}^2) + x\dot{x}) / \dot{y} \qquad \text{(C-4)}$$

Equation (C-4) specifies the locus of points where the time to closest approach is exactly T minutes ahead. Figure C-2 shows the two configurations of this locus of points for the given values of S_1, S_2, x, and $\dot{y}_1$. The shaded areas represent those combinations of $\dot{y}$ and y where $t_{ca}<T$. Being in a shaded region in Figure C-2 is one of the events in (C-1) that determine whether the aircraft pair will be in potential conflict.

The second condition that one has to consider when determining if a potential conflict exists is if the closest approach

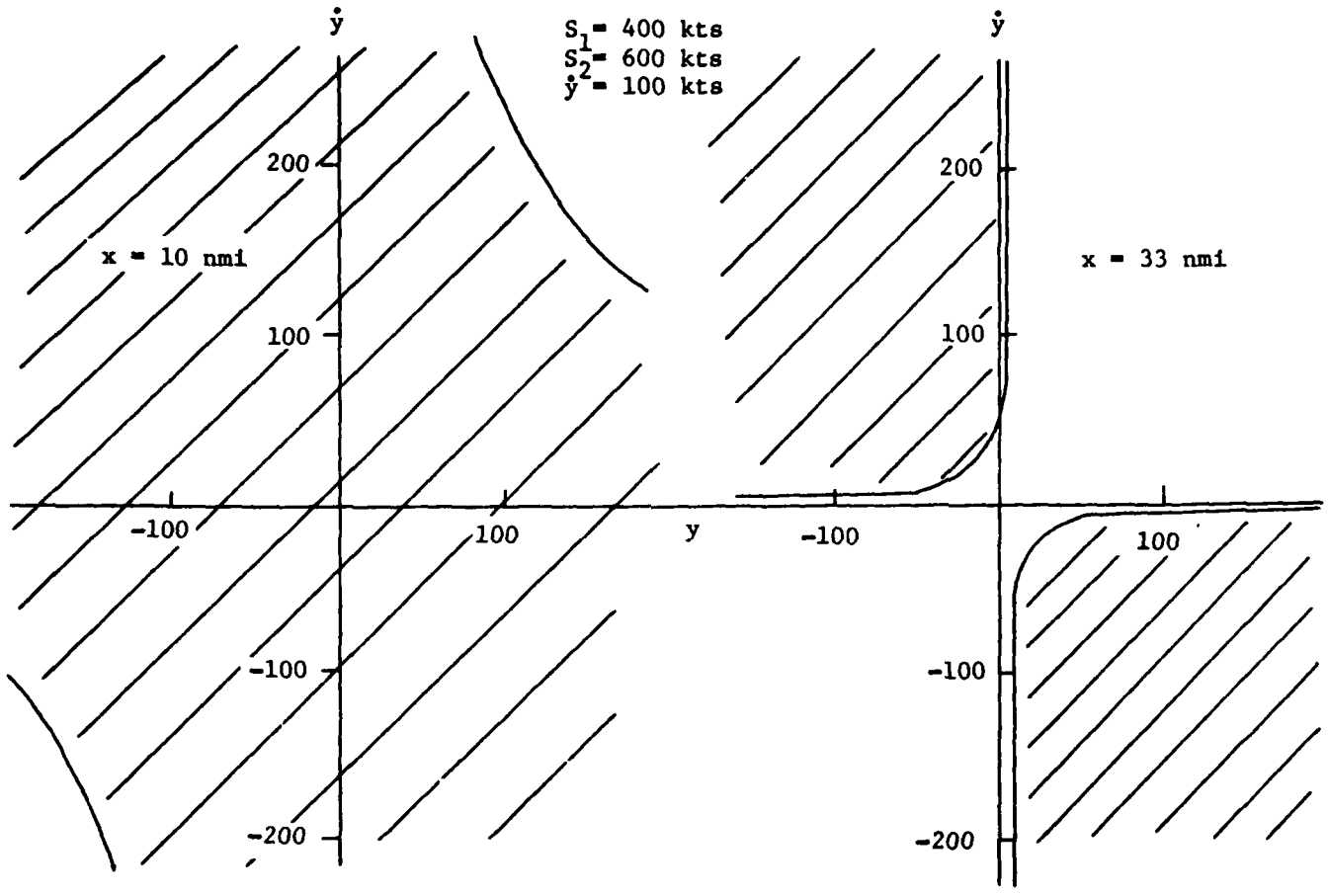

FIGURE C-2
TIME TO CLOSEST APPROACH < T

distance is less than D. This condition is mathematically expressed by substituting t_{ca} as given by (C-3) for t in (C-2) and letting d in (C-2) equal D. After rearranging terms we arrive at

$$y = (-x\dot{y} \pm D\sqrt{\dot{x}^2 + \dot{y}^2})/\dot{x} \qquad \text{(C-5)}$$

Thus, equation (C-5) describes the loci of points where the distance of closest approach is equal to D. Between the two lines described by (C-5) in the y, $\dot{y}$ plane, the closest approach distance is less than D. In terms used in Volume I of this report, this condition defines the "backside" region of the conflict surface.

The third condition specified in (C-1) for a potential conflict is that the separation of the aircraft at the look-ahead time T is less than D. This condition is mathematically described by letting t = T and d = D in equation (C-2). After solving for y we get

$$y = \dot{y}T \pm \sqrt{D^2 - (x + \dot{x}T)^2} \qquad \text{(C-6)}$$

In the y, $\dot{y}$ plane this expression describes two lines. The area between the two lines is where the separation is less than D at time T. This condition defines the "leading edge" region of the conflict surface.

As an illustration of the use of (C-1), (C-4), (C-5), and (C-6) in the determination of the conflict boundary, consider Figure C-3. In this figure the forward speeds of the two aircraft are S_1 = 400 kts, S_2 = 600 kts. Also x = 33 nmi (the alongtrack separation) and $\dot{y}_1$ = 100 kts (the crosstrack speed of aircraft 1). The shaded regions in Figure C-3 defined by lines 4 (corresponding to equation (C-4)) is where the time to closest approach is less than T. The intersection of this region with the region between lines 5 defines where the distance of closest approach is less than D and the time of closest approach is less than T. This is shown by the cross hatched region in Figure C-3.

However, the complete conflict region is given by the union of this region and the region between lines 6. Figure C-4 shows the complete conflict boundary for the given x and $\dot{y}_1$. The maximum extent in $\dot{y}$ for the conflict region is determined by the maximum value of the single aircraft crosstrack speed, in this case 200 kts (200+100 = 300 and -200+100=-100).

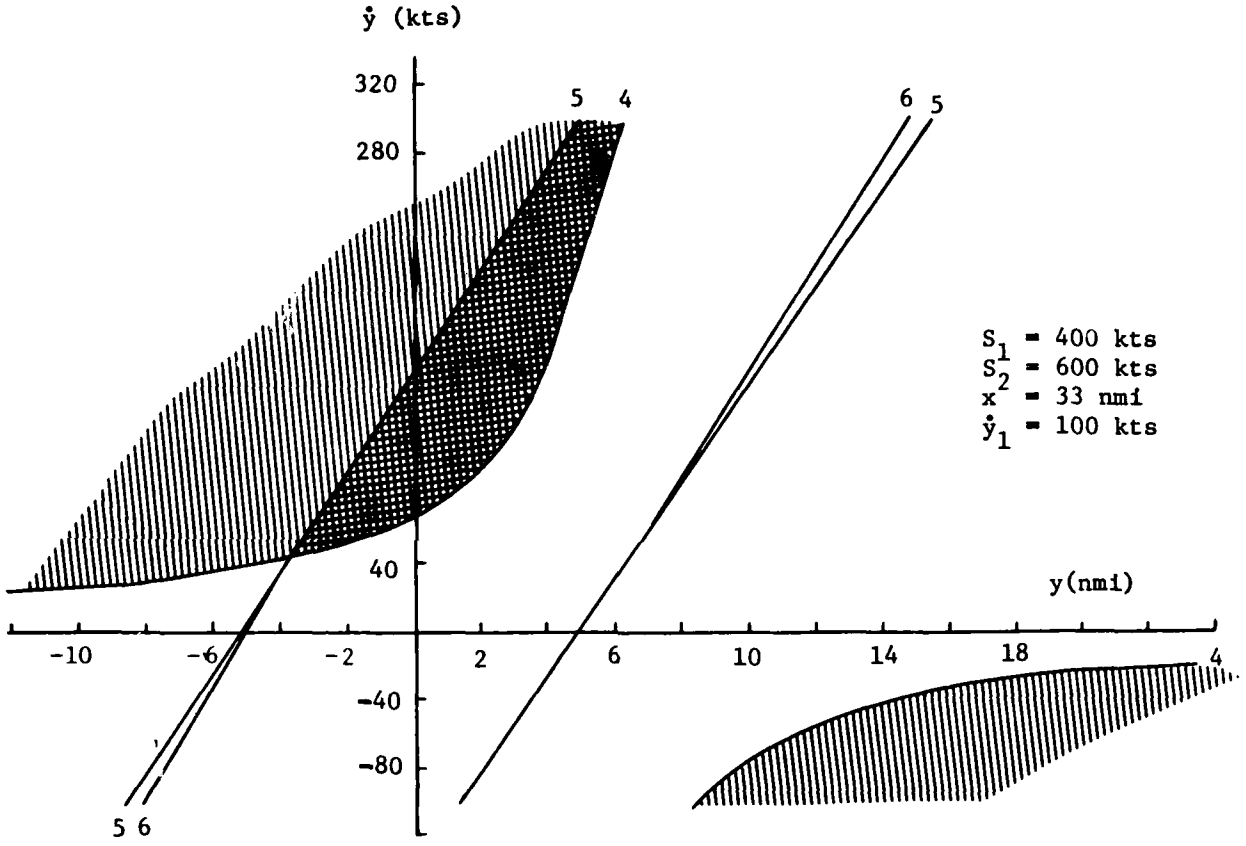

FIGURE C-3
REGIONS OF DISTANCE AT T AND CLOSEST APPROACH TIME AND DISTANCE

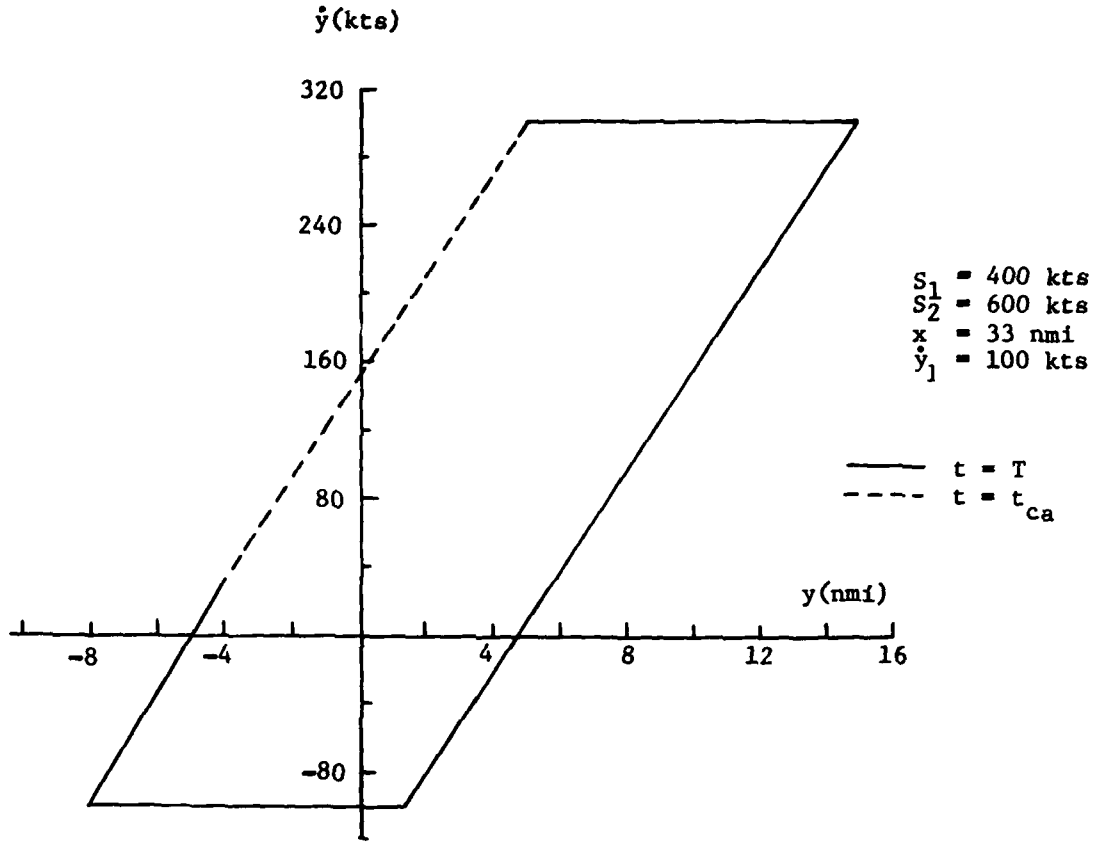

FIGURE C-4
EXAMPLE OF CONFLICT BOUNDARY

It should be obvious from equations (C-4), (C-5), and (C-6) that for various values of x, $\dot{y}_1$, $\dot{y}$, and y either equation (C-5) or (C-6) will determine the boundary. In general, as x becomes small (less than about 28 nmi), lines 6 will not exist because the expression under the radical in equation (C-6) is negative. This means that at exactly 2 minutes in the future the aircraft will have passed each other and would be separated by more than 5 nmi. In this case the conflict boundary is determined by equation (C-5). At larger values of x (greater than about 35 nmi for the given parameter values) there is no intersection between the regions where $t_{ca} < T$ and $d_{ca} < D$. In this case lines 6 determine the conflict boundary. At values of x greater than about 39 nmi the conflict boundary vanishes altogether because the aircraft are too far apart to close within D nmi within T minutes.

In an attempt to graphically display the conflict surface Figure C-5 was produced. This figure shows the top of the conflict surface for one value of $\dot{y}_1$. Due to the computer graphics package used it was not feasible to show that the bottom of the conflict surface is symmetrical with the top. However, Figure C-5 does show the very steep "leading edge" of the conflict surface (larger x) and the shallower "backside" region (smaller x).

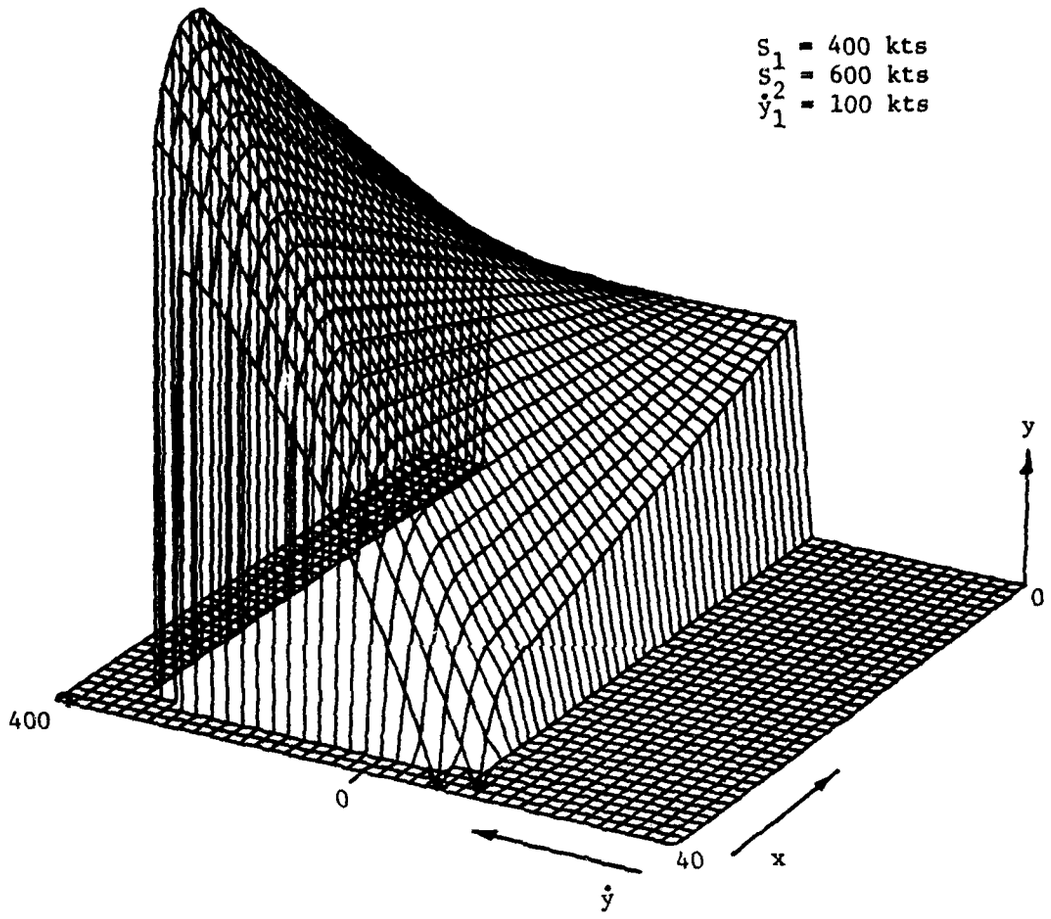

FIGURE C-5
EXAMPLE OF THE TOP HALF OF
CONFLICT SURFACE

APPENDIX D

PENETRATION OF THE CONFLICT SURFACE AND DETECTION DELAYS

This appendix will describe 1) how one can determine where the aircraft pair trajectory will penetrate the conflict surface and 2) how far inside the conflict surface the pair can penetrate before being detected. The basic assumption is that the aircraft pair starts with a large enough initial alongtrack separation that it is not immediately in conflict. Then, based on the particular closing speeds and separations the aircraft pair trajectory may penetrate the conflict surface. As shown in Appendix C the conflict surface has two distinct regions. At large alongtrack separations there is a steep leading edge to the conflict surface in the x-y-$\dot{y}$ space. At smaller values of alongtrack (x) separation the conflict surface is flatter. This is referred to as the backside region. The aircraft pair trajectory will either 1) miss the conflict surface altogether, 2) penetrate the leading edge of the conflict surface, or 3) penetrate the backside region. A trajectory without acceleration can only penetrate the leading edge of the conflict surface. With acceleration the trajectory can penetrate either the leading edge or the backside region. The algorithms for determining the point of penetration of the conflict surface are developed below.

D.1 Leading Edge Penetration

This algorithm is defined using the following parameters: the initial crosstrack separation, the initial crosstrack closing speed, the crosstrack closing acceleration, the initial alongtrack separation, the initial alongtrack closing speed, and the alongtrack deceleration.

D.1.1 Leading Edge Penetration Without Lateral Acceleration

The first step in his algorithm is to assume no accelerations or decelerations and determine if the trajectory of the aircraft pair penetrates the leading edge of the conflict surface. The leading edge of the conflict surface is defined as

$$y = \dot{y}T \pm \sqrt{D^2 - (x+\dot{x}T)^2} \qquad \text{(D-1)}$$

where

y = crosstrack separation

$\dot{y}$ = crosstrack closing speed (+ is closing if $y > 0$)
x = alongtrack separation
$\dot{x}$ = alongtrack closing speed (- is closing)
D = radar minimum separation
T = look ahead time

The trajectory without acceleration as a function of time, t, is given as

$$y = y_o - \dot{y}_o t \qquad (D\text{-}2)$$
$$x = x_o + \dot{x}_o t$$

where $\dot{y}_o$ and $\dot{x}_o$ are the initial crosstrack and alongtrack closing speeds and x_o and y_o are the initial alongtrack and crosstrack positions, respectively. Eliminating t from (D-2) we get

$$y = y_o - \dot{y}_o \frac{x - x_o}{\dot{x}_o} \qquad (D\text{-}3)$$

Substituting (D-3) into (D-1) and solving for x we get

$$x = \frac{-\dot{x}T + x_o(\dot{y}_o/\dot{x}_o)^2 + y_o(\dot{y}_o/\dot{x}_o) - (\dot{y}_o^2 T/\dot{x}_o) \pm \sqrt{DISC}}{1 + (\dot{y}_o/\dot{x}_o)^2} \qquad (D\text{-}4)$$

where

$$DISC = D^2(1+(\dot{y}_o/\dot{x}_o)^2) - ((\dot{y}_o/\dot{x}_o)(x_o - \dot{x}_o T))^2$$
$$-(T + x_o/\dot{x}_o)(2y_o - \dot{y}_o T)\dot{y}_o - y_o(y_o - 2\dot{y}_o T)$$

The conditions that must be met for (D-4) to be a valid solution for the penetration of the leading edge are as follows:

1) DISC must be greater than or equal to zero
2) The larger of the two roots in Equation (D-4) is chosen
3) The chosen root for x must be between zero and x_o

D.1.2 Leading Edge Penetration With Lateral Acceleration

The value of x found from (D-4) is used as the starting value to solve for the penetration of the leading edge with acceleration. The accelerated trajectory is

$$y = y_o - \dot{y}_o t - \ddot{y}\, t^2/2 \qquad (D\text{-}5)$$
$$x = x_o + \dot{x}_o t + \ddot{x}\, t^2/2$$

where the variables are as defined above with the addition of

$\ddot{y}$ = crosstrack acceleration (+ is closing)
$\ddot{x}$ = alongtrack acceleration (+ is decelerating)

The alongtrack acceleration is approximated by assuming that the crosstrack track acceleration is partitioned equally between the acceleration will be constant. This assumption is made to ease the computational complexity and does not introduce too great an error over the parameter ranges of interest. With these assumptions it can be shown that

$$\ddot{x} = \left(\left| \frac{\dot{y}_2}{\dot{x}_2} \right| + \left| \frac{\dot{y}_1}{\dot{x}_1} \right| \right) \frac{|\ddot{y}|}{2} \qquad \text{(D-6)}$$

As the aircraft accelerate the new crosstrack and alongtrack velocities are given by

$$\begin{aligned} \dot{x} &= \dot{x}_o + \ddot{x}t \\ \dot{y} &= \dot{y}_o + \ddot{y}t \end{aligned} \qquad \text{(D-7)}$$

Equations (D-1), (D-5), and (D-7) are used iteratively (as explained below) to solve for t and hence for x, y, $\dot{x}$, and $\dot{y}$.

If there is no real solution to (D-4) or if the accelerations are such that no accelerated penetration of the leading edge takes place, then the possibility of a penetration of the backside of the conflict surface is explored.

D.2 Backside Penetration

The only way for the backside of the conflict surface to be penetrated is with accelerated motion. An accelerated motion trajectory is described by equation (D-5).

The backside of the conflict surface as given in (C-5) is

$$\dot{x}y = -x\dot{y} \pm D\sqrt{\dot{x}^2 + \dot{y}^2} \qquad \text{(D-8)}$$

where $\dot{x}$ and $\dot{y}$ are given in (D-7).

By substituting (D-5) and (D-7) into (D-8) and solving for t one gets the time at which the trajectory penetrates the surface. The method used to solve the non-linear equation is that of Newton where

$$t_n = t_{n-1} - f(t_{n-1})/f'(t_{n-1})$$

where

t_n is the time at the nth interation
$f(\ ) = 0$ is the function whose root is to be found
$f'(\ )$ is the derivative of the function with respect to time.

When a value of t is found that satisfies (D-8) within a stated tolerance, it is substituted into (D-5) and (D-7) to give values for x, y, $\dot{x}$, and $\dot{y}$. Assuming that the lateral acceleration is split equally between the aircraft one can find the new value for $\dot{y}_1$. With these values the conflict geometry is defined. The conflict geometry is valid under the following conditions:

1) x is between zero and x_0 to insure that the aircraft will pass in the future,

2) The absolute value of $\dot{y}_1$ is less than 200 because this is the highest observed lateral velocity, and

3) The absolute value of $\dot{y}$ is less than 400 because this would be the maximum relative lateral velocity.

The procedure outlined above is applied to a set of initial separations and closing speeds. These separations and closing speeds are chosen in the following manner. The initial alongtrack separation is the greatest alongtrack separation at which there is still a possibility of a conflict. This alongtrack separation is given as

$$x_o = (S_1 + S_2) * T+D \qquad \text{(D-9)}$$

where S_1 and S_2 are the forward speeds of the two aircraft, T is the look ahead time and D is the radar separation minimum. The crosstrack separation ranges from -25 to +25 nmi. The minus values indicate that the aircraft have "switched positions" with respect ot their assigned routes. The crosstrack closing speeds range from +400 kts to -400 kts. The minus closing speed indicates an opening situation for positive values of crosstrack separation and a closing situation for negative values of crosstrack separation. Therefore, given an aircraft pair which is separated alongtrack by x_o, crosstrack by y_o, having a crosstrack closing speed of $\dot{y}_o$ while one aircraft has a crosstrack speed of $\dot{y}_1$, and having a relative lateral acceleration, one can determine where on the conflict surface, if at all, the trajectory will penetrate.

D.3 Detection Delays

D.3.1 Methodology

The objective of the detection delay analysis is to estimate a distribution or distributions of the detection delay. This delay is the time it takes to recognize the penetration of a trajectory which is really inside the conflict surface. This estimate was made via simulation. The flow of the simulation proceeded as follows:

1) Randomly choose an initial geometry (i.e. x=35 nmi, y, $\dot{y}$, $\dot{y}_1$ and $\ddot{y}$) and find where the trajectory penetrates the conflict surface as previously described,

2) Select a surveillance/tracker error from a correlated quadrivariate normal distribution (see Appendix B),

3) Add the position and velocity errors due to the surveillance/tracker system to the nominal positions and velocities and check to see whether the observed positions and velocities place the aircraft pair outside the conflict surface,

4) Repeat steps 2) and 3) 100 times and estimate the probability of not detecting the pair within the conflict surface,

5) Estimate the probability of first detecting the pair of aircraft within the conflict surface by taking the product of the probability of detecting the pair inside the conflict surface on this update and the probability of not detecting the pair inside the conflict surface on all the previous updates,

6) Project the trajectory of the aircraft pair ahead over the update time interval,

7) Repeat steps 2) through 6) either 10 times or until the probability of first detection at the current update is less than 10^{-7},

8) Repeat steps 1) through 7) for the given number of replications.

The generation of the surveillance/track errors is based on sampling from a correlated quadrivariate normal distribution. The sampling procedure is explained in Appendix B. The four variables of this distribution are the alongtrack separation, x, the crosstrack separation, y, the alongtrack closing speed, $\dot{x}$, and the crosstrack closing speed, $\dot{y}$. The required transformations to generate the required variates are

$$x = (0.2815U_1 + 0.0821U_2 - 0.02U_3 - 0.06U_4)\,\sigma_x$$

$$\dot{x} = (53.6073U_2 + 5.5U_3 - 11.0U_4)\,\sigma_{\dot{x}}$$

$$y = (0.12U_3 + 0.16U_y)\,\sigma_y$$

$$\dot{y} = (36.0U_4)\,\sigma_{\dot{y}}$$

where U_1, U_2, U_3, and U_4 are four independent normally distributed [N(0,1)] variables. The values of the sigmas are given in Appendix B.

The determination of whether a particular geometry (i.e. set of x, y, $\dot{y}$, $\dot{x}$) is inside or outside the conflict surface is made by basically using the conflict alert algorithm.

D.3.2 Results

The simulation was run for 10 penetration points. The penetration points were randomly chosen with two basic constraints. These constraints were that some penetrations must occur on the leading edge of the conflict surface and some of the penetrations must have significant accelerations. The rest of the penetrations would be backside penetrations and/or have small accelerations (< .015g combined lateral acceleration between the two aircraft). These constraints are based on two hypotheses: 1) that it may be the backside or leading edge penetration position that determines the detection delay and 2) that it may be the magnitude of the acceleration that determines the detection delay.

The results on Table D-1 show that there are 4 leading edge penetrations (the "L" in the LBI column) and 6 backside penetrations. The cumulative histograms of the probability of first detection for each penetration are shown in Table D-2. These cumulative histograms are plotted in Figure D-1. As can be seen the leading edge distribution tends to rise faster than the backside distribution. The reason for this is conjectured

TABLE D-1

SIMULATION PENETRATION POINTS

PENETRATION	CONFLICT GEOMETRY					LBI
	X	Y	Y1DOT	YDOT	YDD	
1	15.59	9.33	103.1	234.4	0.098	B
2	19.17	9.53	94.1	203.5	0.003	B
3	11.39	9.50	178.1	311.5	-0.002	B
4	21.93	5.64	166.6	24.9	0.013	B
5	28.62	7.87	8.1	89.8	0.003	B
6	32.33	6.37	163.4	81.6	-0.008	L
7	30.47	12.91	198.9	250.3	0.004	L
8	32.23	11.46	4.8	255.0	0.063	L
9	28.50	8.89	3.2	121.0	0.035	B
10	31.87	8.88	130.4	19.7	0.040	L

TABLE D-2

CUMULATIVE HISTOGRAMS AT PENETRATION POINTS

UPDATE	PENETRATION									
	1	2	3	4	5	6	7	8	9	10
1	0.5600	0.4900	0.4700	0.5500	0.4500	0.4600	0.3800	0.4300	0.4800	0.4100
2	0.7888	0.7297	0.7668	0.7705	0.6810	0.8326	0.7768	0.8518	0.7192	0.7345
3	0.9307	0.8513	0.8787	0.8875	0.8373	0.9615	0.9330	0.9911	0.8793	0.9416
4	0.9662	0.9331	0.9442	0.9448	0.9284	0.9935	0.9879	0.9997	0.9445	0.9866
5	0.9942	0.9679	0.9710	0.9718	0.9656	0.9992	0.9968	1.0000	0.9778	0.9965
6	1.0000	0.9852	0.9817	0.9879	0.9838	0.9999	0.9994	1.0000	0.9916	0.9996
7	1.0000	0.9941	0.9817	0.9958	0.9930	1.0000	0.9999	1.0000	0.9979	1.0000
8	1.0000	0.9973	0.9817	0.9987	0.9962	1.0000	1.0000	1.0000	0.9998	1.0000
9	1.0000	0.9973	0.9817	0.9997	0.9987	1.0000	1.0000	1.0000	1.0000	1.0000
10	1.0000	0.9973	0.9817	0.9997	0.9995	1.0000	1.0000	1.0000	1.0000	1.0000

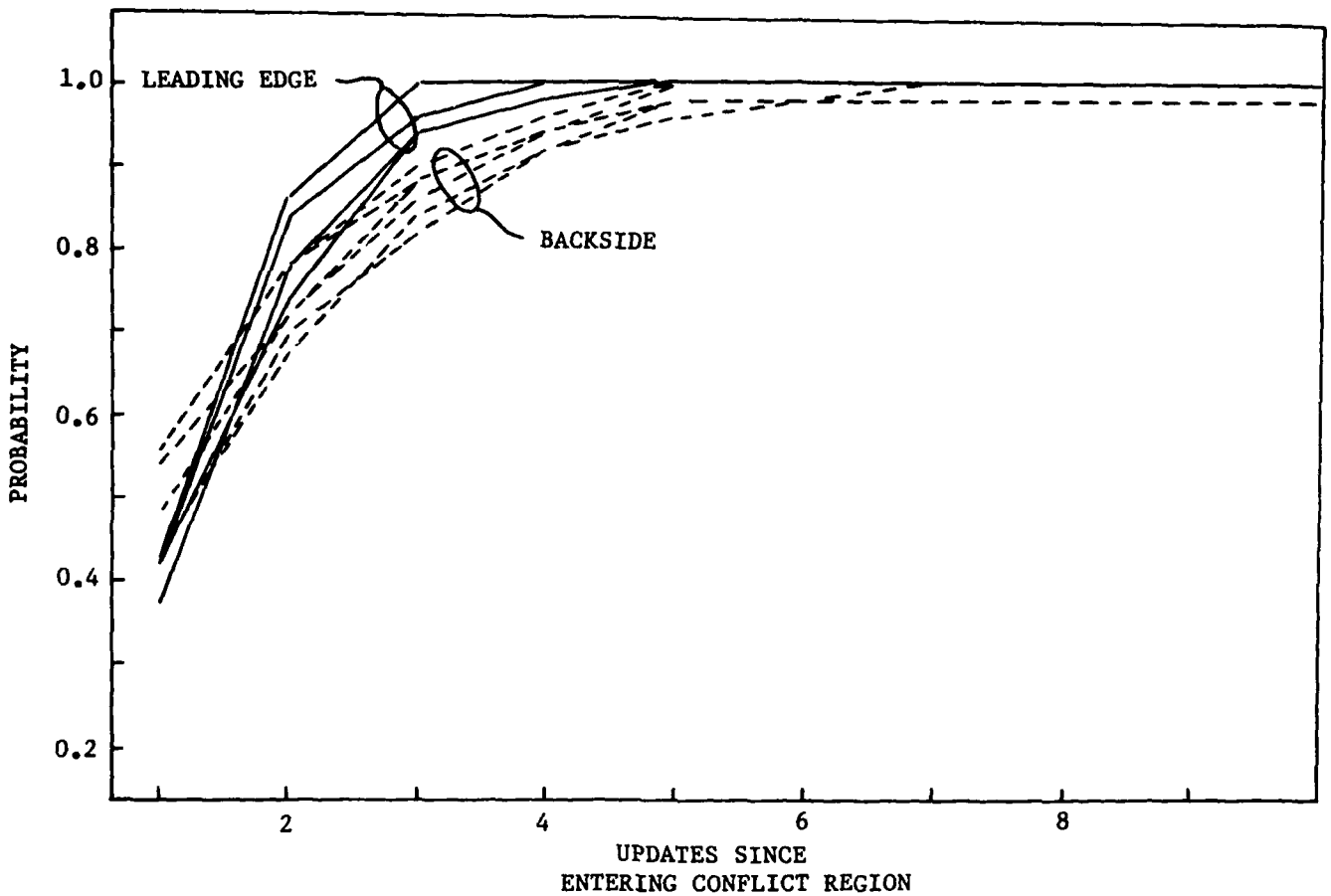

FIGURE D-1
CUMULATIVE DETECTION DELAY DISTRIBUTIONS

to be the following. The leading edge of the conflict surface is curved and thus for an aircraft pair on the surface it is more likely that it appear to be outside the surface. However, after one or two radar updates it is definitely inside the surface and the chances of being detected there quickly become very high. On the other hand, an aircraft pair on the backside with not much acceleration would "slide" down the backside of the conflict surface. At each update there would be approximately a 50-50 chance of detection. Even with acceleration it will take several updates for the aircraft pair to get far enough into the backside of the conflict volume to raise the probability of detection above 0.5 on a given update.

Based on the reasoning above it was decided to assign two detection delays distributions. One is assigned for aircraft pairs entering the leading edge of the conflict surface and one for aircraft pairs entering the backside of the conflict surface. The determination of the detection delay distribution was made by taking the average cumulative probability at each update for the leading edge results and for the backside results. The resulting histograms out to 120 seconds of delay are shown in Table D-3 of the Appendix and in Figure 2-8 in Volume I of this report.

TABLE D-3

DETECTION DELAY HISTOGRAMS

Delay (Sec)	Probability of First Detection	
	Leading Edge	Backside
0	0.4200	0.5000
12	0.3789	0.2443
24	0.1579	0.1307
36	0.0351	0.0716
48	0.0062	0.0315
60	0.0016	0.0138
72	0.0003	0.0054
84	0	0.0018
96	0	0.0006
108	0	0.0002
120	0	0.0001

APPENDIX E

CONFLICT RESOLUTION

E.1 Resolution Algorithm

In the previously modelled resolution maneuver for the same direction case, one of the aircraft was assumed to turn back toward its assigned route. The maximum turn was such that both aircraft were heading in the same direction. It was assumed that after such a turn, the conflict would be over.

In the opposite direction case, it is not necessarily the best maneuver to turn one of the aircraft back to its assigned route. The closing speeds are fast enough that in some cases it is advantageous to turn away from one's route in order to effect a better or even a feasible resolution. Once the direction of turn is decided, there is still the issue of how much to turn the aircraft to resolve the conflict. Surely it is not necessary for the two aircraft to fly parallel courses to resolve the conflict when they originally had opposite courses.

The way the opposite direction resolution maneuver will be handled will be to use the experimental en route Conflict Resolution Advisory algorithm being developed for the FAA. A detailed description of the full algorithm can be found in Reference 4.

Based on the positions and the velocities, the aircraft are projected ahead a given number of seconds (42 seconds is the current parameter) to account for delays and the instantaneous turn to be made by the maneuvering aircraft. After the delay, a wedge of prohibited relative velocity headings is computed for the faster aircraft. This wedge is defined by the vectors UL and UR as shown in Figure E-1. If the relative velocity vector is inside this wedge and the turn is made instantaneously, to take the relative velocity vector outside the wedge, the aircraft will miss by a distance SPR (= 5 nmi).

Now consider that the faster aircraft will be maneuvered. The slower aircraft will have an observed track heading. However, depending on the type of tracking (Free or Flat), there will be errors in the heading of the slower, nonturning aircraft. This is described by a wedge of headings V2L to V2R as shown in Figure E-2 (Aircraft 2 is the nonturning aircraft by

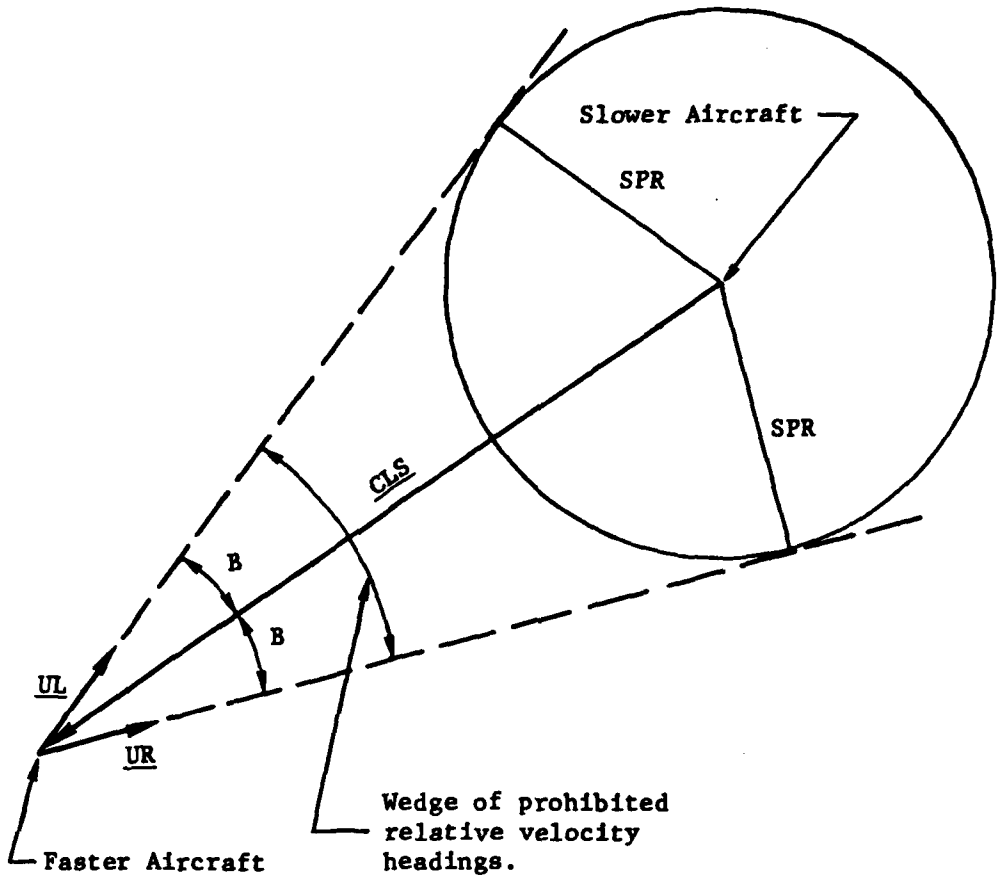

$$\underline{CLS} = (DX, DY)$$

$$DX = XCO\ (FAST) - XCO\ (SLOW)$$

$$DY = YCO\ (FAST) - YCO\ (SLOW)$$

$$CLS = \text{sq rt}\ \left(DX^2 + DY^2\right)$$

FIGURE E-1
PROHIBITED RELATIVE VELOCITY HEADINGS

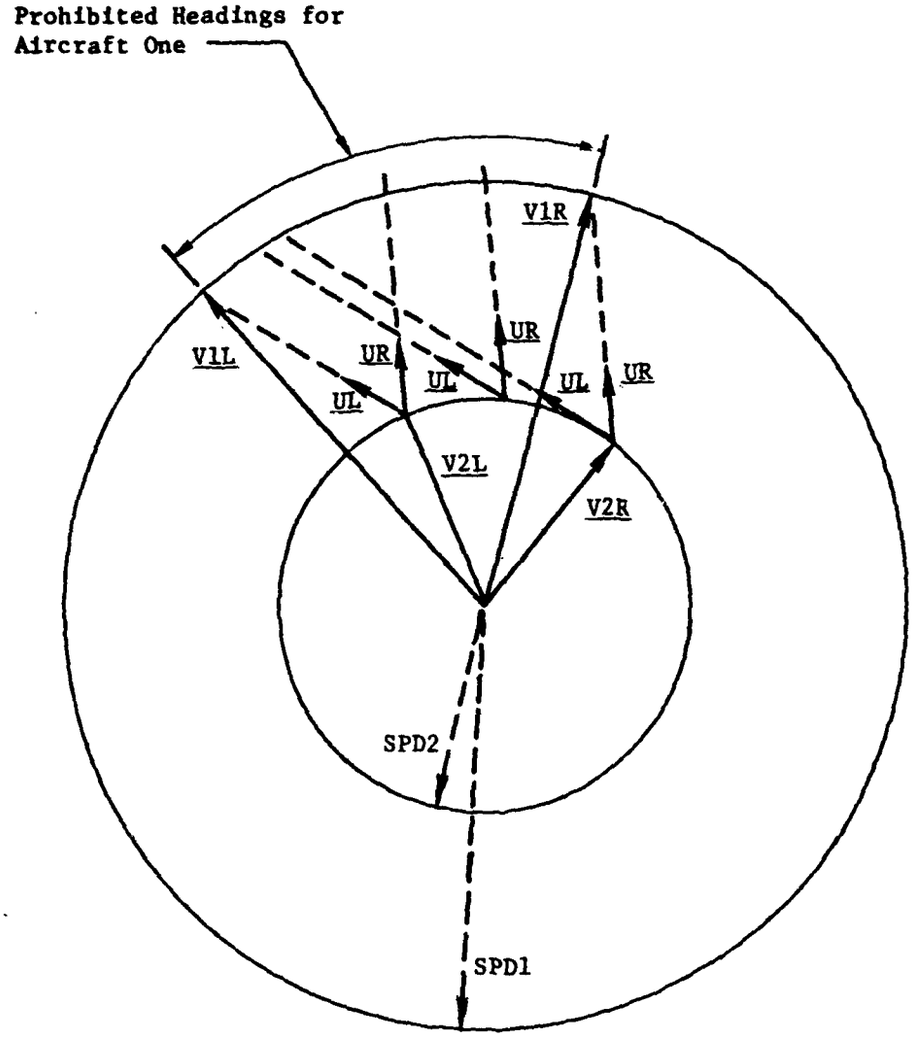

V1L and V1R are computed based on V2L, V2R, UL, UR, SPD1, and SPD2

FIGURE E-2
PROHIBITED HEADING WEDGE
FASTER AIRCRAFT

convention.) The problem is to find the headings for the faster aircraft such that the relative velocity vectors do not fall in the wedge defined by the vectors UL and UR. Figure E-2 depicts the geometry. If the heading of the faster aircraft is to the left of V1L or to the right of V1R no maneuver is required to miss the slower aircraft by SPR. In the algorithm, it is also assumed that the observed heading of the turning aircraft may also be in error so that a given number of degrees is added to V1L and V2R to account for this error. If the heading of the faster aircraft were between V1L and V1R then it would have to turn to the left or right to get its velocity vector out of this wedge.

If one were to turn the slower aircraft the velocity geometry would be as shown in Figure E-3. In this particular case, UL, UR, V2L, and V2R are such that there two prohibited wedges for aircraft 1, the slower, turning aircraft. There could be no prohibited wedge, one wedge, two wedges, or no permitted velocity vector (i.e., the aircraft will not be separated by SPR no matter what the slower aircraft does). Thus, if the slower aircraft's velocity vector is inside a prohibited wedge then it must turn to get its velocity vector out of the wedge. Here again the prohibited wedges are augmented to account for the heading errors of the turning aircraft.

The logic of the Conflict Monitoring Analysis will choose the following maneuver. If neither aircraft's velocity vector is in a prohibtied wedge, then neither is required to make a turn. Otherwise the aircraft which has to make the smallest turn will be the aircraft designated to make the maneuver. It is usually the faster aircraft which will make the maneuver. Thus, both the magnitude and direction of the turn is determined by this algorithm.

If the aircraft are nearly the same speed, one cannot be sure which aircraft is the faster one. In this case, each aircraft is forced, in turn, to be a certain percentage faster than the other. The slower aircraft is maneuvered in each case because this is the more conservative approach (i.e., the slower aircraft will have to turn through a larger angle). The aircraft which is required to turn through the smallest angle when it is forced to be the slower aircraft is chosen to be the turning aircraft.

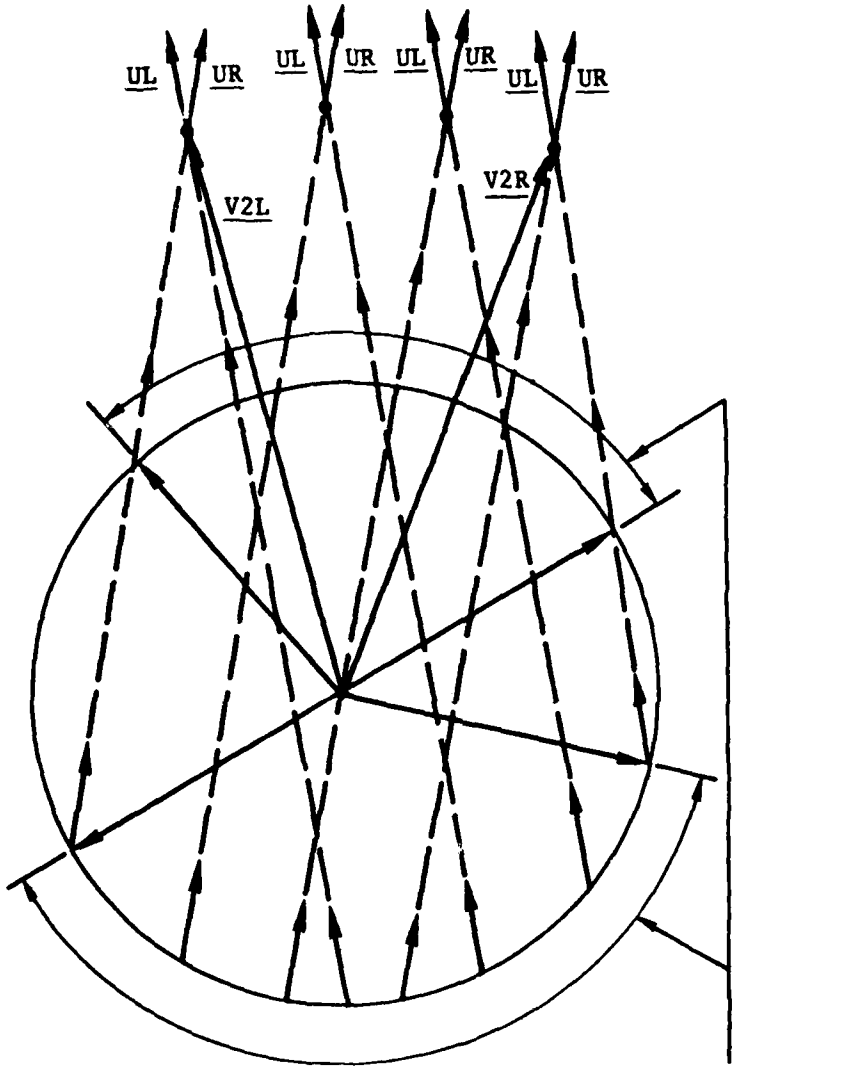

FIGURE E-3
PROHIBITED HEADING WEDGES
SLOWER AIRCRAFT

E.2 Improper Turn Sense Estimates

The resolution advisory algorithm accounts for the uncertainties in the heading errors of the aircraft due to the surveillance/tracker errors by placing wedges about the measured headings of the aircraft. The output from the resolution advisory algorithm tells the controller how far left and how far right one of the aircraft must turn to get out of the conflict situation. In the Conflict Monitoring Analysis it is assumed that the controller will pick the direction of turn to minimize the angle through which the aircraft must turn.

Assume that the true initial configuration of the conflict geometry is known. If this information is used in the Conflict Resolution Advisory algorithm, a decision to turn one of the aircraft right or left is returned. Now, if it is assumed that the surveillance/tracker system estimated the positions and velocities of the aircraft to have values different than the true configuration case, it is possible that the decision from the conflict resolution algorithm could be to turn the aircraft in the opposite sense. It is of interest to the Conflict Monitoring Analysis to be able to estimate the probability of an improper turn sense by knowing something about the true geometry of the conflict.

The object of this investigation is to develop an estimate of the probability of advising the improper turn sense as a function of the conflict geometry.

Characterizing the conflict geometry is best done by considering the logic of the Conflict Resolution Advisory algorithm. That logic is based on a wedge of prohibited headings and the heading of the aircraft to be turned (see Figure E-4). If the heading is nearer to the right (left) boundary of prohibited wedge, the preferred command is to turn right (left). It seems reasonable that if the heading were close to the wedge boundary there would be a high probability of consistently choosing the preferred turn sense. It also seems reasonable that if the heading were in the middle of the prohibited wedge there would be a 50-50 chance that the advisory would recommend either a left or right turn. Based on this argument, a variable is defined which is the ratio of the minimum angle between the aircraft heading and the boundary of the prohibited wedge to the total angle of the prohibited wedge. The value of this ratio will vary from 0 to 0.5.

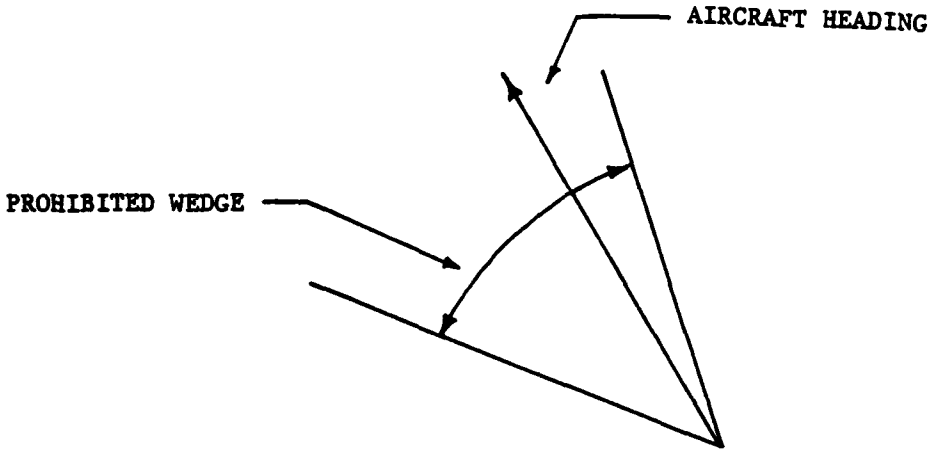

FIGURE E-4
PROHIBITED HEADINGS

The second part of this problem is to estimate the probability of selecting the preferred turn sense as a function of the above defined ratio. This estimate is based on a simulation. The simulation was structured as follows. Initial geometries were chosen at random. These geometries approximated conflict geometries in that it was guaranteed that the time to closest approach was less than 2 minutes and the minimum separation was less than 5 nmi. These geometries represented the "true" geometries of the aircraft pairs. Twenty such geometries were chosen and the Conflict Resolution Advisory was applied to determine the direction of the turn and the value of the ratio. For each "true" geometry a set of position and velocity errors were added to account of the surveillance and tracking system (see Appendix B). These new position and velocity estimates can be regarded as the "perceived" geometries. For each of the "perceived" geometries (there were 50 for each "true" geometry), the Conflict Resolution Advisory was used to determine the direction of the turn. The probability that the turn based on the "perceived" geometries were in the same direction as the turns based on the "true" geometry was estimated as the percentage of turns in the same direction as that advised for the "true" geometry.

It should be stated here that there are four basic outcomes from the Conflict Resolution Advisory when dealing with the "perceived" geometries. They are:

1. The same aircraft gets the same direction turn.

2. The same aircraft gets the opposite direction turn.

3. The other aircraft gets a turn.

4. No aircraft gets a turn.

It was determined from the simulation that in almost all cases, the faster aircraft will get the turn advisory. It is also extremely rare that the other aircraft would get an advisory even due to surveillance/tracker errors. Thus outcome 3 is of no concern. Outcome 4 is also not of concern by definition. It is assumed that the aircraft pair is within the conflict boundary so that this necessitates a turn based on the Conflict Resolution Advisory logic. If the "perceived" geometry leads to

a no turn outcome, then it necessarily follows that the aircraft pair has not yet been perceived within the conflict boundary. The delay in this perception is accounted for in the detection delay analysis discussed in Appendix D.

Thus the conditional probability that the same aircraft receive either the same or opposite direction turns given that a turn is recommended is of interest. The probability of a proper direction turn is shown in Figure E-5. This probability is plotted against the ratio defined above. The points represent outcomes of the simulation. The line is the regression fit to the points. The regression line is

$$y = 1.0888 \sqrt{0.25 - x^2} + 0.45009$$

where y is probability of the proper turn sense and x is the ratio of the minimum angle between the aircraft heading and the boundary of the prohibited wedge to the total angle of the prohibited wedge. The R^2 value of this regression is 0.944.

As one can see from Figure E-5 with the heading near to the edge of the prohibited wedge (Ratio near to zero) the probability is high that the surveillance/tracker error will not cause an improper turn sense to be recommended. However, if the heading is near the middle of the prohibited wedge the surveillance/tracker errors are as likely to advise a turn in one direction as in the other.

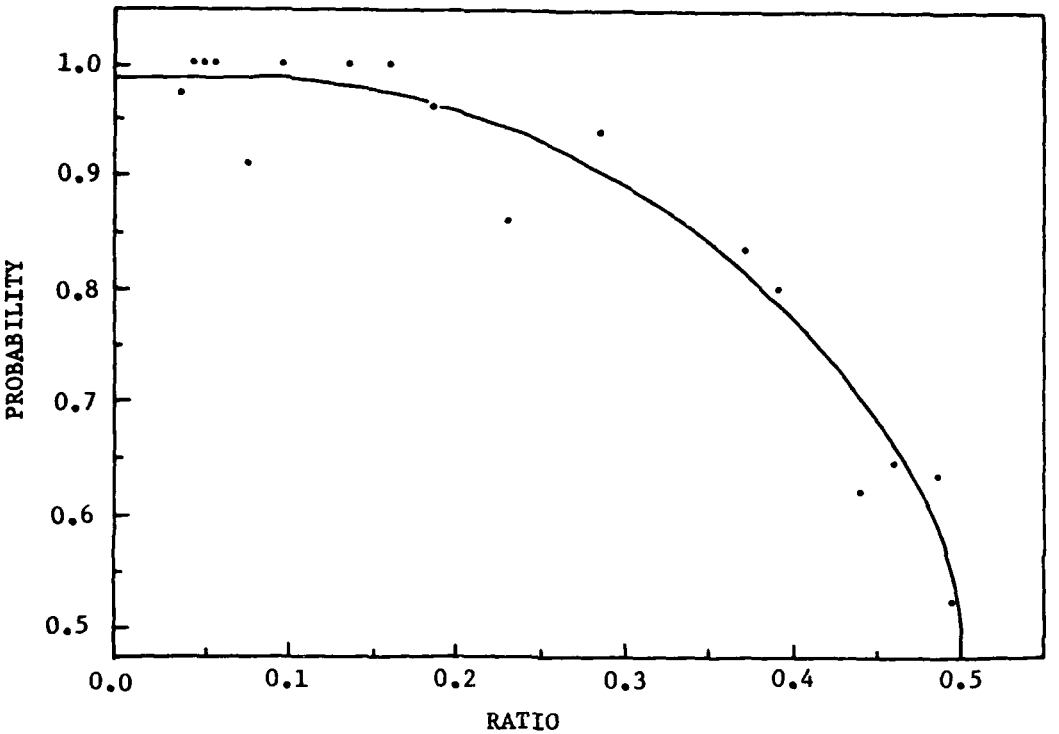

FIGURE E-5
PROBABILITY OF PROPER TURN SENSE
AS A FUNCTION OF "RATIO"

APPENDIX F

OPPOSITE DIRECTION OVERLAP REGIONS

This appendix documents the equations and methods used to compute the overlap regions for opposite direction traffic. The basic difference between this work and that done for the same direction traffic is that accelerations are considered. This, in turn, introduces non-linearities into the equations that were not in the same direction case.

The problem, simply stated, is to find the combinations of delay time and turn rate of one of the aircraft such that an aircraft pair starting with a particular geometry will end in an overlap condition during the course of a single maneuver. If the aircraft are represented as two circles each of radius R, then

$$(x_2(t) - x_1(t))^2+(y_2(t)-y_1(t))^2 \leq (2R)^2 \qquad \text{(F-1)}$$

is the condition of overlap after t seconds. The length of time t is composed of delay time, t_d, and the time in the turn, t_t. Thus

$$t = t_d + t_t \qquad \text{(F-2)}$$

The time in the turn depends on the angle through which the aircraft turns and the turn rate. The angle is denoted as $P|\eta|$ where η is the angle from the Conflict Resolution Advisory algorithm (Appendix E) and P is the fraction of the turn completed before overlap. P ranges from 0 to 1. The sign convention on η is positive for left turns and negative for right turns. The turn rate is denoted as ω. The sign convention for ω is the same as that of η. Thus:

$$t_t = P\left|\frac{\eta}{\omega}\right| \qquad \text{(F-3)}$$

There are certain assumptions used in specifying the acceleration. First the acceleration which is specified is the relative average crosstrack acceleration between the two aircraft. Furthermore, this crosstrack acceleration is assumed to be constant and divided equally between the two aircraft. Another basic assumption in the Conflict Monitoring Analysis is that the forward speeds of the aircraft are also constant. It should be recognized that a constant lateral acceleration and a constant forward speed are inconsistent assumptions. What was done was to adjust the alongtrack track velocity to make the forward velocity nearly constant over the

length of the encounter. It should be noted that the resulting trajectory will not be circular because of the constant crosstrack acceleration.

The expression that is used for the alongtrack velocity, for aircraft i is

$$\dot{x}_i = \dot{x}_{oi} - \frac{\ddot{y}_i t \, (\dot{y}_{oi} + \ddot{y}_i t)}{\dot{x}_{oi}} \qquad \text{(F-4)}$$

where

$\dot{x}_{oi}$ = the initial alongtrack velocity

$\dot{y}_{oi}$ = the initial crosstrack velocity

$\ddot{y}_i$ = the crosstrack acceleration for that aircraft (one-half the relative crosstrack acceleration).

When an aircraft turns its alongtrack velocity will be changed by

$$\frac{V}{\omega} \quad (\cos\xi - \cos(\xi + \omega t_t)) \qquad \text{(F-5)}$$

and its crosstrack velocity will be changed by

$$\frac{V}{\omega} \quad (\sin(\xi + \omega t_t) - \sin\xi) \qquad \text{(F-6)}$$

where

V = the forward speed of the turning aircraft

ξ = the angle between the instantaneous velocity vector at the start of the turn and the positive crosstrack axis. (see Figure F-1)

The definition of ξ is complicated by the acceleration and the fact that it should to be in terms of the initial parameters. After a time delay t_d, the angle ξ is given by

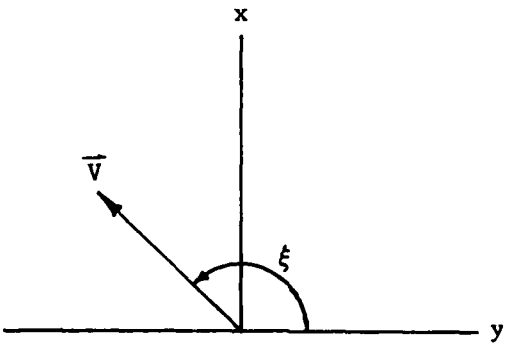

FIGURE F-1
DEFINITION OF ξ

$$\xi(t_d) = \tan^{-1}\left[\frac{\dot{x}_{oi} - \frac{\ddot{y}_i t_d\,(\dot{y}_{oi} + \ddot{y}_i t_d)}{\dot{x}_{oi}}}{\dot{y}_{oi} + \ddot{y}_i t_d}\right] \qquad \text{(F-7)}$$

Combining (F-2), (F-3), (F-4), (F-5) and (F-6) we arrive at

$$\begin{aligned} x_2 - x_1 = {} & x\, t_d \dot{x} - 2A\, t_d t_t - B t_d t_t^2 - (A-D) t_d^2 - B t_d^2\, t_t \\ & -(B-C) t_d^3 + E t_t - A t_t^2 - B\, t_t^3 /3 \\ & \mp \frac{V t_t}{P|\eta|}\left[\cos\xi - \cos(\xi \pm P|\eta|)\right] \end{aligned} \qquad \text{(F-8)}$$

and

$$\begin{aligned} y_2 - y_1 = {} & y + t_d y + y_{02} t_t + (y_2 - y_1)\frac{t_d^2}{2} + y_2 t_d t_t \\ & \mp \frac{V t_t}{P|\eta|}\left[\sin(\xi \pm P|\eta|) - \sin\xi\right] \end{aligned} \qquad \text{(F-9)}$$

where

$$A = \frac{\ddot{y}_2 \dot{y}_{o2}}{2\dot{x}_{o2}}$$

$$B = \frac{\ddot{y}_2}{\dot{x}_{o2}}$$

$$C = \frac{\ddot{y}_1^{\,2}}{\dot{x}_{o1}}$$

$$D = \frac{\ddot{y}_1 \dot{y}_{o1}}{2\dot{x}_{o1}}$$

$$E = \dot{x}_{o2}$$

$\dot{y}_{oi}$ = initial crosstrack speed of aircraft i

$\dot{x}_{oi}$ = initial alongtrack speed of aircraft i

$\ddot{y}_i$ = crosstrack acceleration of aircraft i

$$\dot{x} = \dot{x}_{o2} - \dot{x}_{o1}$$

$$\dot{y} = \dot{y}_{o2} - \dot{y}_{o1}$$

$$x = x_{o2} - x_{o1}$$

$$y = y_{o2} - y_{o1}$$

The top sign is appropriate when $\omega > 0$ while the bottom sign is appropriate when $\omega < 0$. It should be noted that the definitions of the variables are based on the cartesian coordinate system shown in Figure F-1. This convention varies from that used to define the variables in Appendix C.

The ultimate aim is to find those values of t_d and ω which satisfy (F-1). This can be done by considering that (F-1) has the general form of the circle. Therefore (F-1) can be partitioned into two equations by defining a new variable, .

$$x_2 - x_1 - 2R \cos\theta = 0 \qquad (F\text{-}10)$$

$$y_2 - y_1 - 2R \sin\theta = 0 \qquad 0 \leqq \theta \leqq 2\pi$$

There are now two equations and two unknowns. However, (F-10) are nonlinear equations. The solution to these equations is found by using a Newton's iteration technique to solve for t_d and t_t. The value of ω is then found as

$$\omega = \frac{P|\eta|}{t_t}$$

As an example, six values of θ can be chosen. This will yield a region of overlap in $t_d - \omega$ space. One such overlap region is shown in Figure F-2. If one computes the distance between the aircraft as a function of time for the case of $t_d = 13.88$ sec followed by a turn at .19575 deg/sec one finds that the aircraft come within a distance 2R at about 125.7 seconds (see Figure F-3).

Given ranges of x, y, $\dot{y}$, $\dot{y}_1$, and $\ddot{y}$, many of these overlap regions can be computed. The result of doing this for one particular set of such ranges of values is shown in Figure 2-12 in Volume I of this report.

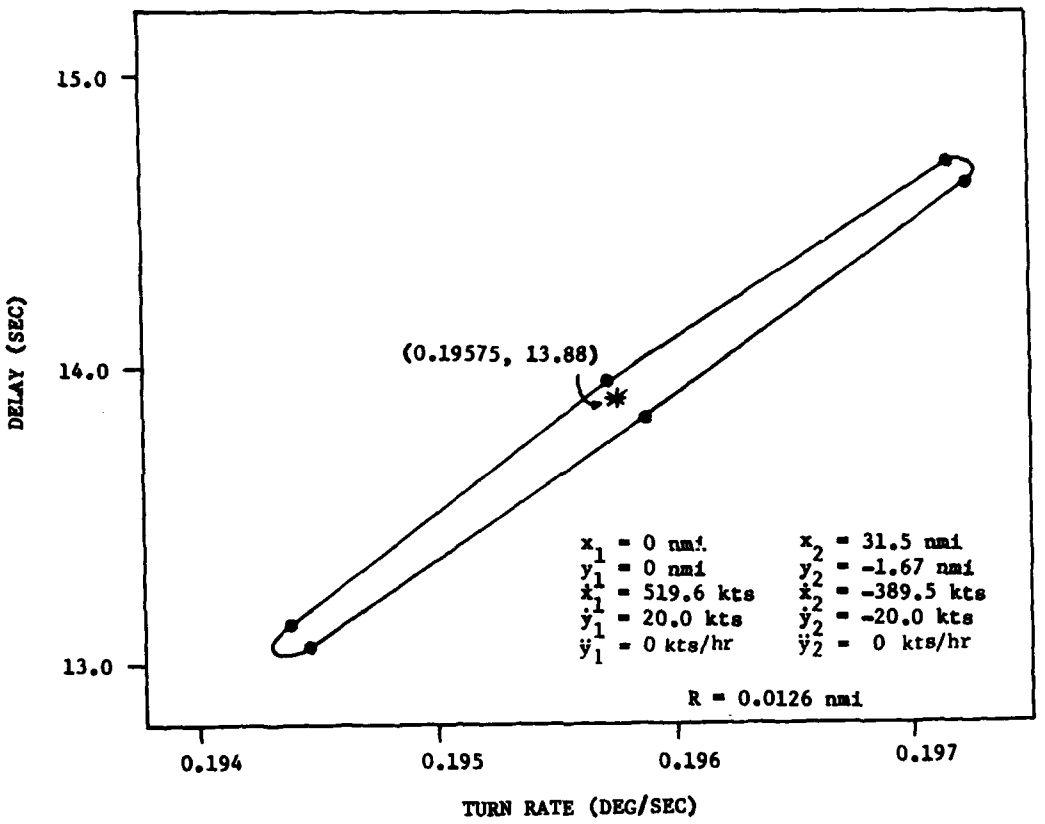

FIGURE F-2
EXAMPLE OF OVERLAP REGION

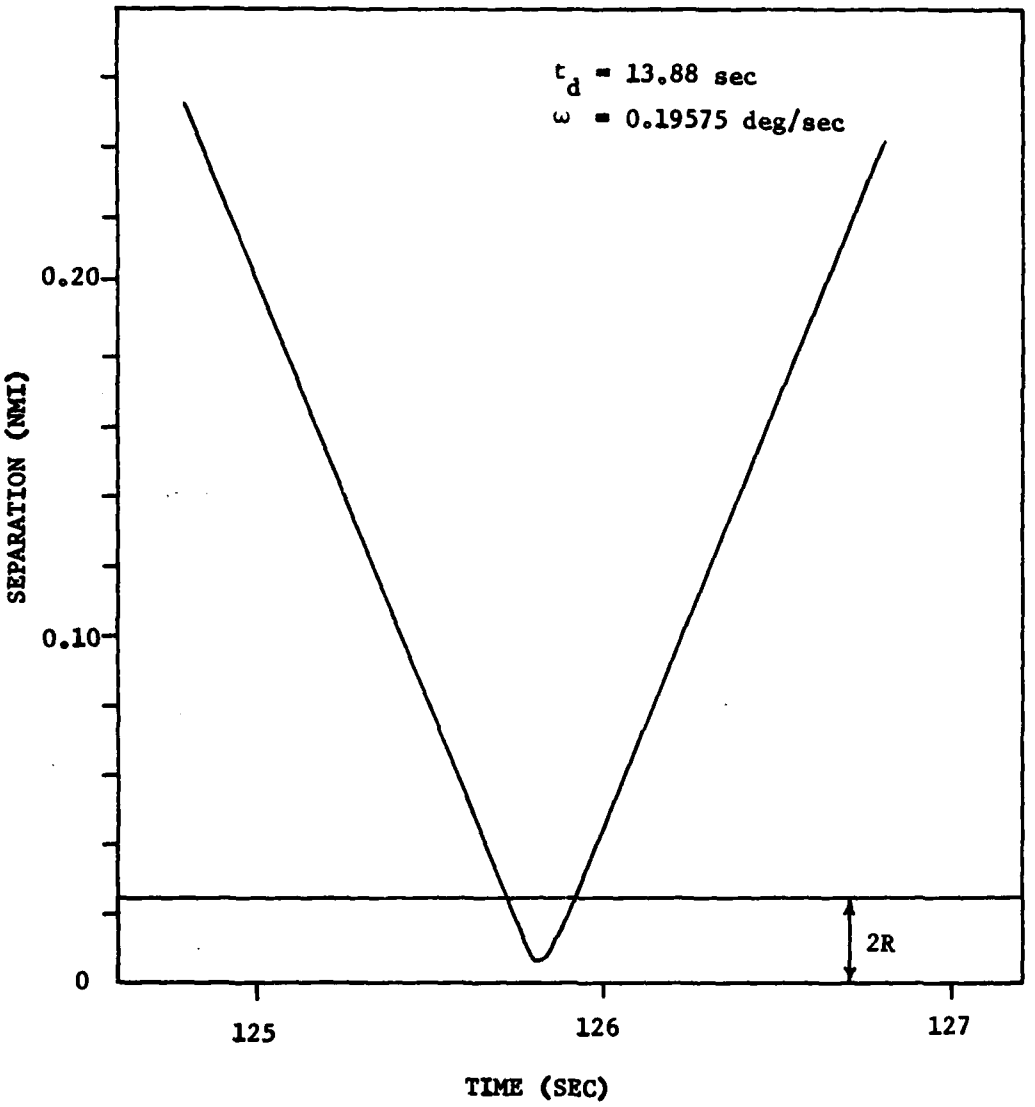

FIGURE F-3
SEPARATION AS A FUNCTION OF TIME

APPENDIX G

PROBABILITY OF HORIZONTAL OVERLAP

In Section 2 of Volume I of this report the procedure for estimating the probability of horizontal overlap was outlined. There was one term in that computational process which is the probability of getting into overlap given that the aircraft pair started in conflict surface cell j. The estimation of this probability is discussed in this appendix.

The estimate of the probability of overlap given the aircraft pair started in cell j is based on the following expression:

$$P(\text{overlap} \mid CS_j) = (P_\ell * P_p + (1-P_\ell)*(1-P_p))*P_{\ell tdo} + ((1-P_\ell)*P_p + P_\ell(1-P_p))*P_{rtdo} \quad \text{(G-1)}$$

where

P_ℓ = probability of left turn command

P_p = probability of proper sense turn

$P_{\ell tdo}$ = probability of left turn, delay, and overlap region

P_{rtdo} = probability of right turn, delay, and overlap region

Each of these probabilities will now be discussed.

From Volume I of this report recall that from a cell on the conflict surface an overlap region in delay/turn rate space can be created. An example of such an overlap region is given in Figure G-1. For the particular region shown both left (positive turn rate) and right (negative turn rate) turns could lead to overlap. In most conflict surface cells only one direction turn will lead to an overlap. To estimate the probabilities $P_{\ell tdo}$ and P_{rtdo} one has to consider the turn rate probability distribution and the total delay probability distribution. One then computes the probability of having a range of turn rates and a range of delay and being in the overlap region. A discussion of the computation of this probability is found in Appendix B of Volume II of Reference 3.

The probability of a left turn command is made by sampling over the conflict surface cell. At each point the Conflict Resolution

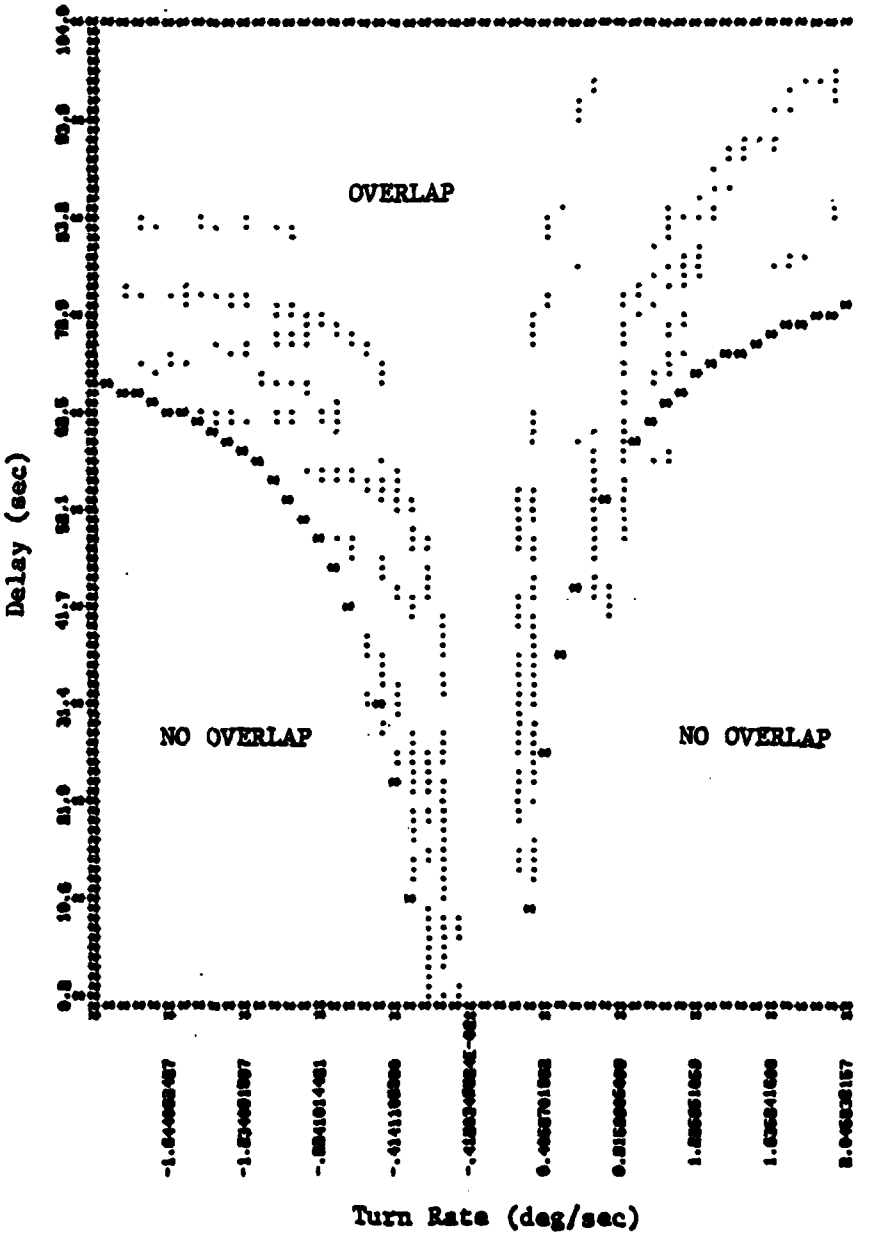

FIGURE G-1
HORIZONTAL OVERLAP REGION

Advisory algorithm is used to indicate whether a right or left turn should be made. The value P is estimated by the fraction of left turn commands from the sample. In most cases for a given conflict surface cell the value of P will be nearly 1 or nearly 0. It is also true that in most cases the predominant turn direction is away from the overlap situation. This indicates that with good surveillance information the proper turn direction is given by the Conflict Resolution Advisory.

The term P_p is the probability that the proper turn direction is in fact given to the pilot. An improper turn direction would be due to surveillance/tracker error. The estimate of P_p is based on the heading of the turning aircraft with respect to the wedge of prohibited headings given in the Conflict Resolution Advisory algorithm (see Appendix E). From a simulation it was found that if the aircraft heading were near the middle of the prohibited wedge of headings (see Figure G-2) the chances are 50-50 that the improper turn sense would be selected by the Conflict Resolution Advisory algorithm. If the aircraft's heading were near the edge of the prohibited wedge of headings the chances are remote that the surveillance errors would cause an improper turn sense. A simulation was performed to arrive at an estimate of the probability of the Conflict Resolution Advisory algorithm selecting the proper turn sense as a function of the position of the aircraft heading within the wedge of prohibited headings. This simulation is discussed in Appendix E. The result is that

$$P_p = 1.0888 \sqrt{0.25 - R^2} + 0.45009$$

where R is the ratio of the angle through which the aircraft is to turn to the total angle covered by the prohibited wedge.

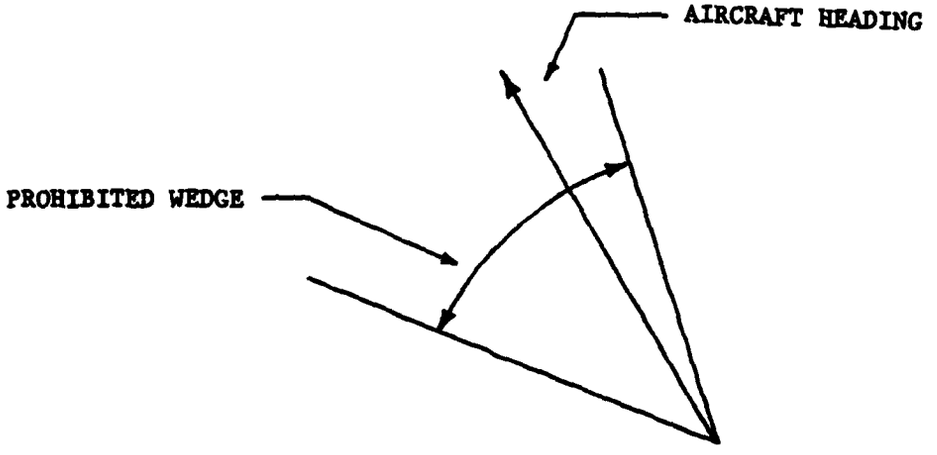

FIGURE G-2
PROHIBITED HEADINGS

APPENDIX H

REFERENCES

1. Smith A. P., "Interim Report on the Conflict Monitoring Analysis of Parallel Route Spacing in the High Altitude CONUS Airspace with Opposite Direction Traffic Flows." The MITRE Corporation, WP-81W00362, Volume I, McLean, Va., June 1981.

2. Reinsch, C. H. "Smoothing by Spline Functions." Numerische Mathematik, Volume 10, pp. 177-183, 1967.

3. Smith A. P., "Interim Report on the Conflict Monitoring Analysis of Parallel Route Spacing in the High Altitude CONUS Airspace." The MITRE Corporation, FAA-EM-80-16, Volume I and Volume II, McLean, Va., July 1980.

4. Hauser, S. J. et al, "En Route Conflict Resolution Advisories: Functional Design Specification Coordination Draft." The MITRE Corporation, MTR-80W00137, McLean Va., April 1980.

5. "Preliminary Recommendations Concerning Improvements to the Current Methodology for Spacing Parallel Jet Routes in a Strictly Strategic Air Traffic Control Environment." FAA Technical Center, Radio Technical Commission for Aeronautics Paper No. 292-79/SSRG-36, Atlantic City, N. J. November 1979.

MITRE Department
and Project Approval: Balraj G. Sokkappa

Dr. Balraj G. Sokkappa

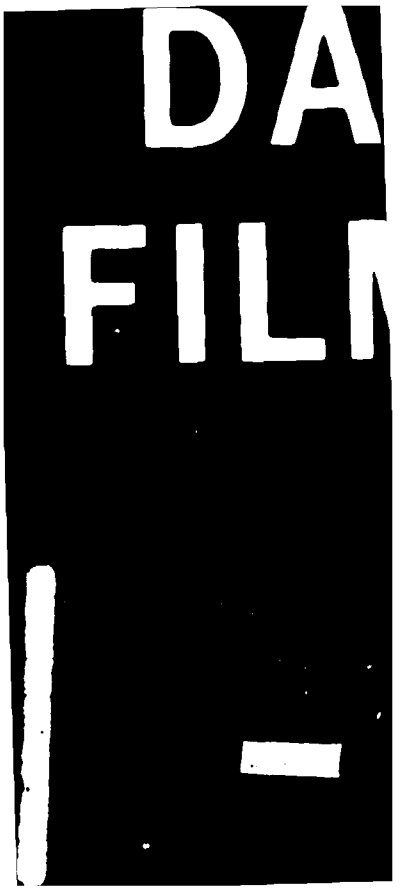
DA
FIL